JCI The Journal of Clinical Investigation

Mutations affecting the conserved acidic WNK1 motif cause inherited hyperkalemic hyperchloremic acidosis

Helene Louis-Dit-Picard, … , Juliette Hadchouel, Xavier Jeunemaitre

J Clin Invest. 2020. https://doi.org/10.1172/JCI94171.

Research In-Press Preview Genetics Nephrology

Gain-of-function mutations in the *WNK1* and *WNK4* genes are responsible for Familial Hyperkalemic Hypertension (FHHt), a rare inherited disorder characterized by arterial hypertension and hyperkalemia with metabolic acidosis. More recently, FHHt-causing mutations in the KLHL3-CUL3 E3 ubiquitin ligase complex have shed light on the importance of WNKs cellular degradation on renal ion transport. Using full exome sequencing in a four-generation family and then targeted sequencing in other suspected cases, we have identified new missense variants at the *WNK1* gene, clustering in the short conserved acidic motif known to interact with the KLHL3-CUL3 ubiquitin complex. Affected subjects had an early-onset and a marked hyperkalemic phenotype, but normal blood pressure values. Functional experiments in *Xenopus laevis* oocytes and HEK293T cells demonstrated that these mutations strongly decrease the ubiquitination of the kidney-specific isoform KS-WNK1 by the KLHL3-CUL3 complex, rather than the long ubiquitous catalytically active L-WNK1 isoform. A corresponding CRISPR-Cas9 engineered mouse model recapitulated both the clinical and biological phenotype. Renal investigations showed increased activation of the SPAK-NCC phosphorylation cascade, associated with impaired ROMK apical expression in the distal part of the renal tubule. Altogether, these new *WNK1* genetic variants highlight the importance of the KS-WNK1 isoform abundance on potassium homeostasis.

MUTATIONS AFFECTING THE CONSERVED ACIDIC WNK1 MOTIF CAUSE INHERITED HYPERKALEMIC HYPERCHLOREMIC ACIDOSIS

Hélène LOUIS-DIT-PICARD[1,2,£], Ilektra KOURANTI[1,2,£], Chloé RAFAEL[1,2,3,4,£] Irmine LOISEL-FERREIRA[1,2,£], Maria CHAVEZ-CANALES[1,2,5], Waed ABDEL-KHALEK[1,2], Eduardo R. ARGAIZ[6,7], Stéphanie BARON[2,8], Sarah VACLE[9], Tiffany MIGEON[3], Richard COLEMAN[10], Marcio DO CRUZEIRO[11], Marguerite HUREAUX[12], Nirubiah THURAIRAJASINGAM[12], Stéphane DECRAMER[13], Xavier GIRERD[14], Kevin O'SHAUGNESSY[15], Paolo MULATERO[16], Gwenaëlle ROUSSEY[17], Ivan TACK[18], Robert UNWIN[19], Rosa VARGAS-POUSSOU[12], Olivier STAUB[9], Richard GRIMM[10], Paul A. WELLING[10], Gerardo GAMBA[6,7], Eric CLAUSER[1,2], Juliette HADCHOUEL[1,2,3], Xavier JEUNEMAITRE[1,2,12]§

AFFILIATIONS

1. INSERM, PARCC, F-75015 Paris, France.
2. Université de Paris, Paris, France.
3. INSERM UMR_S1155, Tenon Hospital, Paris, France
4. Université Paris-Diderot, Sorbonne Paris Cité, Paris, France
5. Translational Medicine Unit, Instituto de Investigaciones Biomédicas, Universidad Nacional Autónoma de México and Instituto Nacional de Cardiología Ignacio Chávez, Tlalpan, México City.
6. Molecular Physiology Unit, Instituto de Investigaciones Biomédicas, Universidad Nacional Autónoma de México and Instituto Nacional de Ciencias Médicas y Nutrición Salvador Zubiran.
7. Tecnológico de Monterrey, Escuela de Medicina y de Ciencias de la Salud, Monterrey, NL, México.
8. Service d'Explorations Fonctionnelles, AP-HP, F-75015 Paris France
9. Department of Pharmacology and Toxicology, University of Lausanne, Lausanne, Switzerland.
10. Department of Physiology, University of Maryland School of Medicine, Baltimore, Maryland
11. INSERM U1016, Institut Cochin, Paris, France
12. Assistance Publique Hôpitaux de Paris (AP-HP), Département de Génétique, Hôpital Européen Georges Pompidou, Paris, 75015, France.
13. Service de Néphrologie Pédiatrique, Hôpital des Enfants, Toulouse, France.
14. Assistance Publique Hôpitaux de Paris (AP-HP), Institute of Cardiometabolism and Nutrition (ICAN) - Unité de Prévention Cardiovasculaire - Hôpital de La Pitié-Salpêtrière, Paris France.
15. Department of Medicine, University of Cambridge, CAMBRIDGE, United-Kingdom.
16. Division of Internal Medicine and Hypertension Unit, Department of Medical Sciences, University of Torino - TORINO, Italy.
17. Néphrologie Pédiatrique - Clinique Médicale Pédiatrique, Hôpital Mère Enfant - CHU de Nantes - NANTES, France
18. Service des Explorations Fonctionnelles Physiologiques, CHU de Toulouse et INSERM U1048 - I2MC, TOULOUSE, France.
19. UCL Department of Renal Medicine, University College London, Royal Free Campus and Hospital, LONDON, United-Kingdom.

[£] These authors contributed equally to the work

§ **Corresponding author:**
Xavier Jeunemaitre
INSERM U970, Centre de Recherche HEGP, PARCC
56, rue Leblanc 75015 Paris, France
Tel: + 33 1 5398 8023; Fax: + 33 1 5398 7952
E-mail: xavier.jeunemaitre@inserm.fr

Key Words: WNK kinases, kidney, ion transport, blood pressure

Summary

Identification and functional characterization in cellular and animal models of WNK1 mutations highlighting the role of its kidney-specific isoform on potassium metabolism

ABSTRACT (198 words)

Gain-of-function mutations in the *WNK1* and *WNK4* genes are responsible for Familial Hyperkalemic Hypertension (FHHt), a rare inherited disorder characterized by arterial hypertension and hyperkalemia with metabolic acidosis. More recently, FHHt-causing mutations in the KLHL3-CUL3 E3 ubiquitin ligase complex have shed light on the importance of WNKs cellular degradation on renal ion transport. Using full exome sequencing in a four-generation family and then targeted sequencing in other suspected cases, we have identified new missense variants at the *WNK1* gene, clustering in the short conserved acidic motif known to interact with the KLHL3-CUL3 ubiquitin complex. Affected subjects had an early-onset and a marked hyperkalemic phenotype, but normal blood pressure values. Functional experiments in *Xenopus laevis* oocytes and HEK293T cells demonstrated that these mutations strongly decrease the ubiquitination of the kidney-specific isoform KS-WNK1 by the KLHL3-CUL3 complex, rather than the long ubiquitous catalytically active L-WNK1 isoform. A corresponding CRISPR-Cas9 engineered mouse model recapitulated both the clinical and biological phenotype. Renal investigations showed increased activation of the SPAK-NCC phosphorylation cascade, associated with impaired ROMK apical expression in the distal part of the renal tubule. Altogether, these new *WNK1* genetic variants highlight the importance of the KS-WNK1 isoform abundance on potassium homeostasis.

INTRODUCTION

Familial Hyperkalemic Hypertension (FHHt), also known as Gordon syndrome and Pseudohypoaldosteronism type 2, is a rare disease associated with net positive Na^+ balance and renal K^+ retention, resulting in hypertension, hyperkalemia and hyperchloremic metabolic acidosis (1). Mutations causing FHHt were first identified in the *WNK1* and *WNK4* genes that encode two members of the WNK (With No lysine (K)) serine-threonine kinase family (2). More recently, we and others have identified disease-causing mutations in the Kelch-like 3 (KLHL3) and Cullin 3 (CUL3) proteins belonging to an ubiquitin-protein ligase complex (3, 4). This complex has been shown *in vitro* to interact with WNK1 and WNK4, induce their ubiquitination and regulate their protein level through proteasomal degradation (5-8). Ohta and collaborators mapped the interaction site in WNK1 to a region containing a short acidic motif, which is highly conserved among the members of the WNK family (5). Interestingly, most of the FHHt-causing *WNK4* variants cluster in this motif and are charge-changing. WNK4 proteins carrying the same mutations fail to interact with the KLHL3 adaptor protein *in vitro* (5-7). This causes increased WNK4 abundance with secondary activation of the Na^+-Cl^- co-transporter (NCC) and development of FHHt (6, 7).

The genetic heterogeneity of FHHt is reflected in its phenotypic heterogeneity, ranging from severe cases presenting in childhood to mild and sometimes asymptomatic cases presenting in late-adulthood (9, 10). A similar spectrum exists for the more recent causal genes, *KLHL3* and *CUL3*, with *CUL3* mutations causing the most severe hypertension and electrolyte abnormalities (3). A milder phenotype was suggested for the WNK1-FHHt cases that could be partly explained by a different mutational mechanism. Indeed, the *WNK1* gene gives rise to two main isoforms: a long ubiquitously expressed and catalytically active isoform (L-WNK1) and a short kidney-specific isoform (KS-WNK1), which is only expressed in the distal nephron (11, 12). FHHt-causing *WNK1* mutations were found to be large deletions located in intron 1, resulting in an increased expression of L-WNK1 in the distal convoluted tubule (DCT) and connecting tubule (CNT) (13).

We have now identified cases and families with inherited hyperkalemic hyperchloremic acidosis carrying missense variants in the *WNK1* gene that all cluster in the conserved acidic motif and are similar to those found previously in *WNK4*. Affected subjects had a clear electrolyte phenotype but no significant BP increase, especially in comparison with those who had similar *WNK4* mutations. Their functionality was tested in *Xenopus* oocytes and HEK293T cells, showing that they mainly affect the regulation of KS-WNK1 by the KLHL3-CUL3 ubiquitin complex. Using the CRISPR/Cas 9 genome editing system, a mouse line was created that replicated the human phenotype and which was used to analyze the consequences of mutations at the WNK1 acidic motif on renal transport.

RESULTS

A missense variant in the WNK1 acidic motif in the first FHHt kindred

We took advantage of one four-generation family to combine linkage analysis and whole exome sequencing (WES). This family included seven affected individuals (all with metabolic acidosis and hyperkalemia, but with

normal BP) and six unaffected individuals (Figure 1A and Supplemental Table 1A). Using a SNP-based linkage approach, seven suggestive linkage regions (maximum logarithm of odds (LOD) score = 1.8 in all linked regions) were identified in this panel (Supplemental Table 1B). In total, linked regions spanned 69 Mb and included 829 protein-coding genes. After filtering, WES performed in one unaffected and two affected individuals identified 71 possible new coding-causing disease variants (Supplemental Table 1C). Four missense variants mapped to the linkage regions and were predicted *in silico* to be damaging. These variants were located in *SLC30A7* (solute carrier family 30 member 7, a zinc transporter), *KIF11* (kinesin family member 11), *TCTN3* (tectonic family member 3) and *WNK1* (With No lysine (K) 1). The *WNK1* variant (c.1905T>A; p.Asp635Glu (Figure 1B)) was located in exon 7 (ex7) that encodes the conserved acidic motif, previously shown to mediate the interaction with the substrate adaptor KLHL3 (14).

Additional variants in the WNK1 acidic motif in other cases and kindreds

FHHt-causing *WNK4* mutations are located in exons 7 and 17, encoding highly conserved acidic and basic motifs, respectively. Thus, we screened the homologous motifs of WNK1 encoded by exons 7 and 25, respectively, in twenty-six unrelated affected cases, previously found as negative for the classical mutations in *WNK4, KLHL3, CUL3*, or the intron 1 deletion in *WNK1*. Direct sequencing identified five additional non-synonymous heterozygous variants in ex7 in eight unrelated subjects (Figure 2A-C). The *in silico* pathogenicity of these variants is described in Supplemental Table 2. All were located within the acidic motif, between position 631 and 636 of the L-WNK1 protein, and were predicted to be pathogenic. Four of the six missense variants were charge-changing (E631K, D635N, Q636R, Q636E); two affected residues (D635, Q636) were also found mutated in the homologous acidic motif of *WNK4* (D564 and Q565, Figure 2C-D)

Clinical and biochemical characteristics: hydrochlorothiazide-sensitive hyperkalemic acidosis without hypertension

Detailed clinical and biological characteristics of index cases are given in Table 1. The circumstances of discovery and the clinical symptoms of these index patients are detailed in the Supplemental Table 3. In most of the cases, patients were asymptomatic and showed with no signs of hyperkalemia on an electrocardiogram. All displayed the electrolyte anomalies typical of FHHt, including marked hyperkalemia (median 5.9 mmol/L; IQR 5.3-6.3), hyperchloremia (median 108 mmol/L; IQR 106-110) and metabolic acidosis (Total CO_2 20 mmol/L; IQR 19-21), despite a normal GFR (median creatinine 58 micromol/L; IQR 47-74). For the seven index cases with prospective reliable clinical data, hyperkalemia and hyperchloremia were rapidly corrected with low doses of hydrochlorothiazide (6.25 to 25 mg/day; Supplemental Figure 1). By comparison, an average drop in potassium of only 0.7 mmol/L is observed in normal healthy subjects administered a much higher dose of HCTZ (50 mg, 3 weeks) (15). Compared to reference values (16), we also observed a tendency for significant hypercalciuria in infancy and adulthood (Supplemental Figure 2).

Surprisingly, most of the index cases had casual BP values in the normal range, except a 25-year old woman with associated obesity (K3-1, BMI 32 Kg/m^2) and a 22-year old woman (K88-1) without other cardiovascular risk

factors but who had short stature and mild mental retardation (Table 1). This tendency for normal BP values was confirmed in the first-degree relatives harbouring the familial mutations, since only 2/10 were mildly hypertensive (Supplemental Table 4). Overall, the 20 mutated individuals with measured BP (23 ±18 years) belonging to 9 affected families had normal systolic (116 ±20 mmHg) and diastolic BP (73 ± 21 mmHg). Low or suppressed plasma renin levels were observed with normal to slightly elevated plasma aldosterone concentrations (Table 1, Supplemental Table 4), as have been observed with other FHHt genotypes.

We then compared the clinical phenotypes of FHHt patients with *WNK1* ex7 missense mutations with those who had *WNK4* missense variants affecting the same acidic motif collected in our centre and in the literature (Table 2). Interestingly, WNK4-related patients consistently had the strongest BP and electrolyte phenotype, whatever the sub-classification (index cases, adults or males only); BP was much higher in patients with WNK4 mutations (SBP and DBP averaged ~20 mmHg and ~10 mmHg higher) compared to patients with *WNK1* ex7 mutations.

The WNK1 ex7 mutations selectively abolish the ubiquitination and degradation of the KS-WNK1 isoform in vitro

The acidic motif common to WNK1 and WNK4 has been reported as a binding site for the CUL3 and KLHL3 E3-ubiquitin ligase complex (14). Therefore, we tested the effect of KLHL3 on the abundance of wild-type and mutant L- and KS-WNK1 isoforms (Figure 3). The expression of KLHL3 in *Xenopus laevis* oocytes resulted in a small (about 30%), but significant, decrease in the amount of L-WNK1 and almost completely abolished KS-WNK1. We then analyzed the recurrent *WNK1* A634T variant, found in the K58, K75 and K88 kindreds. No significant change in L-WNK1 abundance was observed between the wild-type and mutant isoforms, whereas the KS-WNK1-A227T mutant was highly expressed in comparison with the wild-type KS-WNK1 isoform, suggesting that the mutation abrogates the degradation of KS-WNK1 (Figure 3A). We also tested the other observed WNK1 missense variants of the acidic motif using the same experimental system (Supplemental Figure 3A). All were protective with regard to KLHL3/CUL3 mediated degradation.

Since both WNK1 isoforms are physiologically co-expressed in the distal nephron (12), we sought to characterize how KLHL3/CUL3 mediated degradation affects KS- and L-WNK1 abundance in co-expression experiments (Figure 3B). On KLHL3 expression, a 70-80% decrease in wild-type KS-WNK1 abundance was observed while there was no change in L-WNK1. This major difference was not observed after transfection with the mutated isoforms. The co-expression of wild-type and mutant isoforms lead to an intermediate decrease in KS-WNK1 abundance, suggesting that only the wild-type KS-WNK1 was degraded. Overall, these results suggest that human mutations of the WNK1 acidic motif selectively increase KS-WNK1 abundance in the distal nephron where KLHL3 is exclusively expressed.

We also tested the effect of KLHL3 on the wild-type and mutant WNK1 isoforms, in human tissue culture HEK293T cells. Since we found that this cell line expresses high levels of CUL3 but undetectable levels of KLHL3, we first established a stable tetracycline-inducible cell line expressing KLHL3 (see Supplemental methods). The induction of KLHL3 resulted in a dramatic decrease in the level of transfected KS-WNK1 but not

L-WNK1 (Figure 4A). The introduction of the D635N mutation (D228N for the KS-WNK1 isoform) prevented this decrease. Interestingly, all other mutations were also protective with regard to KLHL3/CUL3 mediated degradation with the exception of KS-WNK1 D228E (Supplemental Figure 3B). The substitution of an aspartic acid (D) by a glutamic acid (E) is not charge-changing, which might explain the milder phenotype. The co-expression of L- and KS-WNK1 in HEK293T cells confirm the observations made in Xenopus oocytes (Figure 4B). Next, we immunoprecipitated L- and KS-WNK1 and assayed their ubiquitination status in denaturing conditions to exclude any ubiquitination signal linked to WNK1 interactors. KLHL3 induction resulted in heavy KS-WNK1 ubiquitination whereas it had little or no effect on L-WNK1 or D635N (D228N) mutants (Figure 4C). KS-WNK1 ubiquitination by the KLHL3/CUL3 complex suggests that the E3 ligase adaptor (KLHL3) and the substrate (WNK1) interact. Indeed, both L-WNK1 and KS-WNK1 co-immunoprecipitate KLHL3 in native conditions. However, KS-WNK1 does so with a much higher efficiency (Figure 4D). As expected, the D635N mutation in the acidic domain (D228N in KS-WNK1) reduced the interaction with KLHL3. Taken together, our *in vitro* studies strongly suggest that KS-WNK1 is the preferential WNK1 isoform target of the KLHL3/CUL3 ubiquitin-complex and that the mutations identified in *WNK1* ex7 prevent this ubiquitination.

A mouse model bearing a mutation at WNK1 acidic motif confirms the absence of arterial hypertension despite a typical electrolyte phenotype

To understand why *WNK1* ex7 missense mutations lead to a hyperkalemic metabolic acidosis with normal blood pressure in most of the affected patients, we sought to generate a mouse model bearing the D635E mutation at the WNK1 acidic motif using the CRISPR/Cas9 genome editing technology (Supplemental Figure 4A). The knock-in of the point mutation was not found in 300 microinjected oocytes but an in-phase suppression of a GAA triplet leading to the deletion of the first amino acid of the WNK1 acidic motif (delE631) was observed in 7/300 injected oocytes, (Supplemental Figure 4B). *In vitro*, this mutant had a similar effect to the reference D635N variant, abrogating the KLHL3-induced decrease in KS-WNK1 abundance (Supplemental Figure 4C). The analysis of the blood pressure and plasma electrolytes concentration confirmed that the heterozygous *Wnk1*$^{+/delE631}$ mice represent an adequate model in which to study the *in vivo* consequences of the *WNK1* mutations identified in our patients.
Using telemetry, we found that systolic and diastolic BP were similar in heterozygous *Wnk1*$^{+/delE631}$ mice and wild-type littermates (Figure 5A). Tailed-cuff measured systolic BP on a larger set of adult males also revealed the absence of hypertension (113 ±5 mmHg, n=20 *Wnk1*$^{+/delE631}$ vs 108 ±5 mmHg, n=20 *Wnk1*$^{+/+}$, ns). The homozygous *Wnk1*$^{delE631/delE631}$ delE631 mice were perfectly viable with no departure from the expected mendelian proportions when heterozygous mice were crossed. The biological phenotype of these homozygous mice did not differ from the heterozygous mice, with the exception of SBP, which was significantly higher than in heterozygous or wild-type littermates when measured by tailed-cuff (Supplemental Table 5). We focused our studies on the heterozygous model since it corresponds to the human autosomal dominant pathology.
Wnk1$^{+/delE631}$ mice displayed hyperkalemia (5.1 ± 0.5 mmol/L) and hyperchloremia (114 ±2 mmol/L) (Figure 5B) that were corrected by a 3-day hydrochlorothiazide oral administration (Table 3). Urinary aldosterone excretion was increased 2-fold whereas renin expression was decreased by 45% in *Wnk1*$^{+/delE631}$ mice (Table 3 and Supplemental Table 6). This difference remained significant after a 7-day low K^+ diet and normalisation of

kalemia (Figure 5C), suggesting that the lower renin is probably the consequence of a mild volume expansion rather than the hyperkalemic state (17). To better appreciate the absence of hypertension in this model, we performed BP telemetry measurements in *Wnk1*$^{+/delE631}$ and *Wnk1*$^{+/+}$ male littermates (6-7 months old) on a 1-week normal standard diet (0.3% NaCl) followed by a 1-week high NaCl (3%) diet (Figure 5A, right panel). The results confirm that there was no difference in basal BP between the two groups (systolic BP: 124.5 ±10.4 in *Wnk1*$^{+/+}$ vs 125.2 ±8.4 mmHg in *Wnk1*$^{+/delE631}$), as well as no significant BP increase on a high sodium diet (systolic BP: 120.6 ±10.1 in *Wnk1*$^{+/+}$ vs 128.1 ±10.1 mmHg in *Wnk1*$^{+/delE631}$; Supplemental Table 6).

Increased activation of the SPAK-NCC phosphorylation cascade.

The extreme sensitivity of FHHt patients to thiazide diuretics initially suggested that the syndrome resulted from an increased activity of the Na^+-Cl^- cotransporter NCC. This hypothesis was confirmed by the demonstration that NCC abundance and phosphorylation are increased in all FHHt mouse hypertensive models (13, 18-20). Despite the absence of arterial hypertension, we observed the same phenomenon in the renal cortex of *Wnk1*$^{+/delE631}$ mice compared with *Wnk1*$^{+/+}$ littermates (Figure 6). The SPAK (Ste20 Proline Alanine rich Kinase) kinase is essential for the expression and phosphorylation of NCC *in vivo* (20, 21). Immunoblotting on whole-kidney cortex homogenates showed that SPAK phosphorylation is greater in *Wnk1*$^{+/delE631}$ mice, compared to *Wnk1*$^{+/+}$ (Figure 6). We also observed an increased abundance of the full-length SPAK isoform, which is the one predominantly expressed in the DCT (22), as well as a significant increase in OSR1 (Oxidative Stress-Responsive kinase 1). WNK4 abundance was not significantly changed in the kidney of *Wnk1*$^{+/delE631}$ mice (Figure 6). However, due to the lack of a suitable antibody, we could not measure the phosphorylation level of the T-loop serine, which reflects the activation state of the kinase (23).

To further characterize the activation of the WNK1-SPAK/OSR1 cascade in the kidney of *Wnk1*$^{+/delE631}$ mice, we performed immunofluorescence experiments with an antibody recognizing both L- and KS-WNK1 isoforms (a KS-WNK1 specific antibody is not available). While the DCT of *Wnk1*$^{+/+}$ mice contained small WNK1-positive puncta, large WNK1-positive structures, resembling the previously described WNK bodies, were observed in *Wnk1*$^{+/delE631}$ NCC-positive DCTs (Figure 7). These bodies were also found in some AQP2-positive but not in NKCC2-positive tubules. Previous studies demonstrated that KS-WNK1 is required for the formation of these WNK1 bodies, which are dynamic membraneless structures (24). Containing the components of the WNK/SPAK pathway, they are usually not present at baseline conditions but form under conditions of low potassium intake when WNKs become activated (25). The fact that we observed them at baseline in *Wnk1*$^{+/delE631}$ kidneys provides further support that the WNK1/SPAK cascade is activated in *Wnk1*$^{+/delE631}$ mice.

Potassium Secretory Capacity is Diminished without change of ENaC expression in *Wnk1*$^{+/delE631}$ *Mice*

Basal urinary K^+ excretion and urinary/plasma ratio of K^+ concentration was lower in *Wnk1*$^{+/delE631}$ mice indicating a defect in urinary potassium excretion (Figure 8A-B). We calculated the transtubular potassium gradient (TTKG) to estimate the potassium secretory capacity of the aldosterone sensitive distal nephron (ASDN, connective tubule and collecting duct) (26). *Wnk1*$^{+/delE631}$ mice exhibited significantly lower TTKG (8.6 ±0.3, n=24) than *Wnk1*$^{+/+}$

mice (10.1 ± 0.3, n=24, p=0.0003), despite higher aldosterone levels, consistent with a potassium secretory defect (Figure 8C). As observed in patients, HCTZ rapidly corrected the hyperkalemia in the *Wnk1*$^{+/delE631}$ mice (see above) and partially abolished the TTKG difference between the *Wnk1*$^{+/+}$ and *Wnk1*$^{+/delE631}$ mice (Figure 8C), suggesting the defect develops as a consequence of increased Na^+ reabsorption by NCC and reduced sodium delivery to ASDN. Metolazone, a thiazide diuretic suggested to have less carbonic anhydrase inhibitory effect, did not correct the phenotype when administered intraperitoneally at the dose of 50 µg/Kg.day during 4 days (Supplemental Figure 5).

Decreased activity of the Epithelial sodium (Na) Channel ENaC and the Renal Outer Medullary potassium (K) channel ROMK are thought to contribute to the hyperkalemia in other forms of FHHt (27). Abundance of ENaC α- and γ-subunits in the membrane-enriched fraction of the renal cortex was assessed as a surrogate for channel function (28, 29). No significant increases in the abundance in full-length or cleaved forms of the ENaC subunits were observed *Wnk1*$^{+/delE631}$ mice compared to *Wnk1*$^{+/+}$, excepted for the short fragment of α subunit (Figure 8D). We then acutely treated *Wnk1*$^{+/delE631}$ and *Wnk1*$^{+/+}$ mice with amiloride, the specific pharmacological inhibitor of ENaC. Six hours after the amiloride injection, the natriuresis increased very significantly and similarly in both groups that had similar Na and K intake (Figure 8E). Urinary K^+ excretion decreased also similarly in *Wnk1*$^{+/+}$ and in *Wnk1*$^{+/delE631}$ (Figure 8F), the difference in post-amiloride absolute values reflecting the difference in basal values. Together these results make it unlikely that alterations in ENaC contribute to the potassium secretory defect.

Altered Regulation of ROMK in *Wnk1*$^{+/delE631}$ Mice

We then analysed ROMK expression in the kidney cortex and at the apical pole of the distal part of the DCT (DCT2) and CNT cells, where the channel is most significantly upregulated in response to dietary potassium loading (30). At the basal level, western blots showed that ROMK protein expression was not increased in *Wnk1*$^{+/delE631}$ mice compared to *Wnk1*$^{+/+}$ littermates despite significant hyperkalemia (5.1 ±0.1 vs 4.4 ±0.1). By contrast, a significant increase in ROMK abundance was observed in wild-type mice when a similar rise in plasma potassium was induced by amiloride administration (Figure 9A). Immunofluorescence experiments revealed that apical ROMK expression was not modified in either the DCT2 and CNT of the hyperkalemic *Wnk1*$^{+/delE631}$ mice compared to normokalemic *Wnk1*$^{+/+}$ mice (Figure 9B). This lack of ROMK increase in the distal nephron is considered as abnormal in these hyperkalemic *Wnk1*$^{+/delE631}$mice.

We also studied the expression of large-conductance Ca^{++}-activated K^+ (BK) channel which expression was unchanged. Likewise, the protein abundance of the Na-K-2Cl cotransporter (NKCC2) co-transporter (Figure 9C, D), which has been shown to be regulated *in vivo* by KS-WNK1 (31), was unchanged, a significant increase in NKCC2 phosphorylation was observed (Figure 9D), in accordance with the observed increase in SPAK and OSR1, the main kinases involved in the phosphorylation of NKCC2 (32), and opposite of the expected inhibitory effect KS-WNK1. We did not detect an increase in KS-WNK1 in NKCC2-positive tubules (Figure 7), suggesting other regulatory mechanisms are at play (33).

DISCUSSION

This is the first report of missense mutations in the *WNK1* gene leading to an autosomal dominant tubulopathy. The syndrome is striking in that it resembles more an isolated form of hyperkalemic renal distal tubular acidosis than a classic FHHt. Our cases are very similar to the three published cases of Spitzer-Weinstein syndrome, characterized by normotension and early-onset hyperkalemic tubular acidosis, and sensitive to hydrochlorothiazide (34-36). The mutations are all located in the acidic motif, which is highly conserved across members of the WNK family and pivotal for their recruitment by KLHL proteins for ubiquitination by the CUL3-based E3 ligase ubiquitin complex (5, 37). Our *in vitro* experiments suggest that *WNK1* mutations result in a differential regulation of the two major WNK1 isoforms, with an increase in abundance of KS-WNK1 being preferentially affected compared with the kinase active L-WNK1.

Since the discovery that mutations in *KLHL3* and *CUL3* cause FHHt (3, 38), several studies have demonstrated that the WNK kinases are substrates for the KLHL3-CUL3 E3 ligase complex (37). Ohta et al mapped the WNKs interaction site to a region containing a motif of ten amino acids "EPEEPEADQH", called the acidic motif because of the predominance of negatively charged residues (5). Most of the FHHt-causing mutations in WNK4 cluster in this highly conserved motif (2). The analysis of the Kelch domain of KLHL3 crystal structure in complex with the WNK4 acidic motif revealed close polar contacts between several residues at this motif and other conserved residues at the surface of the Kelch domain beta-propeller (14). In particular, the D635 residue of L-WNK1 (equivalent to D564 in WNK4) establishes ionic interactions with R528 of KLHL3, both residues being mutated in FHHt. Mutations in this degron motif abolish the interaction of WNK4 with the ubiquitin-ligase complex, thereby preventing their ubiquitination and proteasomal degradation. Accordingly, WNK4 protein abundance increases in the kidney of $WNK4^{+/D561A}$ mice, which carried one of the FHHt mutations (7, 39).

We found that KS-WNK1 abundance is much more affected by the acidic motif mutations than L-WNK1. While the expression of KLHL3 only slightly reduced L-WNK1 abundance, the expression of KS-WNK1 was drastically decreased in both *Xenopus laevis* oocytes and mammalian cells (HEK293T). We also found that KS-WNK1 is more ubiquitinated than L-WNK1 when KLHL3 is overexpressed. Each of the mutations in the acidic motif abolished the degradation of KS-WNK1, with the exception of KS-WNK1 D228E. Ohta et al. previously demonstrated that L-WNK1 interacts with KLHL3 and that this interaction is prevented by mutations in either KLHL3 or the acidic motif of L-WNK1 (5). However, the effect of KLHL3 overexpression on KS-WNK1 abundance and ubiquitination was not tested. Therefore, the potential difference in sensitivity of WNK1 isoforms to KLH3-induced degradation was not analyzed. The acidic motif is present in both L- and KS-WNK1 isoforms. Thus, one might have expected that the missense mutations would have the same consequence on both isoforms. However, the two proteins have a different 3D-structure, the conformation of which is probably regulated by different factors. Piala et al. showed that L-WNK1 is maintained in an inactive conformation by the binding of chloride to the catalytic site (39). KS-WNK1 is insensitive to this regulation, because it lacks the major part of the kinase domain. Under physiological conditions, KS-WNK1 mRNA is markedly more abundant than L-WNK1

in the distal nephron (13, 40), but data on KS-WNK1 protein abundance is still lacking since there are no specific antibodies against this isoform. Our results obtained in both *Xenopus* oocytes and HEK293T cells suggest that KS-WNK1 protein could be physiologically degraded in the distal nephron by ubiquitination through the KLHL3-CUL3 E3 ligase complex.

The present study suggests that mutations in the WNK1 acidic motif drive altered potassium metabolism primarily by increasing KS-WNK1 abundance. The most parsimonious explanation for the phenotype is that the selective increase in KS-WNK1 abundance directly stimulates NCC activity and abrogates potassium-dependent upregulation of ROMK. The explanation is consistent with recent observations indicating that KS-WNK1 is critical for the coalescence of WNK-SPAK signalling molecules into large membraneless structures in the DCT, called WNK bodies (24), which appear to be key intermediates in WNK-SPAK phosphorylation of NCC, particularly during dietary potassium restriction (41). Because binding of KS-WNK1 to WNK4 increases the phosphorylation of the WNK4 T-loop (23) and the WNK bodies become larger in DCT of $Wnk1^{+/delE631}$ mice, we speculate that increased abundance of KS-WNK1 in $Wnk1^{+/delE631}$ mice drives phosphorylation of NCC through the activation of the WNK4-SPAK cascade in the WNK bodies. As evidenced by the rapid correction of hyperkalemia in $Wnk1^{+/delE631}$ mice and patients with HCTZ, the aberrant activation of NCC most likely contributes to urinary potassium retention by reducing sodium delivery to ASDN.

The fact that an increased KS-WNK1 abundance stimulates NCC expression and phosphorylation in the $Wnk1^{+/delE631}$ mice might be considered surprising given that the same phenomenon was observed in mice carrying an inactivation of KS-WNK1 (*KS-*$Wnk1^{-/-}$ mice, (42)). However, given the information raised in the last ten years, we now believe that increased NCC activity in *KS-*$Wnk1^{-/-}$ mice is not directly caused by KS-WNK1 inactivation but is rather the consequence of the potassium-losing phenotype. The latter could be caused by the increased ROMK expression observed in the DCT2/CNT of these mice and associated with a decrease in aldosterone secretion in the absence of decreased renin expression. This new interpretation is supported by the fact that all the other mouse models in which NCC is stimulated display hypertension and hyperkalemia (Wnk4-PHAII transgenic mice (19), $WNK4^{D561A/+}$ knockin mice (18), $KLHL3^{-/-}$ mice (43), $KLHL3^{R582/+}$ mice (44) and constitutively active SPAK mutant mice (45)). In addition, our original interpretation of the phenotype resulting from KS-WNK1 inactivation (42) was guided by the early oocyte studies, which suggested that this WNK1 isoform exerted a dominant negative effect on L-WNK1 (46). However, we have since shown that an unfortunate mutation in the L- and KS-WNK1 cDNA used in these oocyte studies caused spurious loss-of-function (47). A newer study in oocytes, using the corrected cDNA, now indicates that KS WNK1 in an activator of WNK4 (48).

Based on our observation that $Wnk1^{+/delE631}$ mice fail to properly upregulate ROMK in the setting of hyperkalemia, it seems likely that KS-WNK1 inhibits pathways that normally up-regulate ROMK in the DCT2/CNT, and this contributes to the potassium retention phenotype. This conclusion is consistent with observations in mice that KS-WNK1 gene ablation causes apical membrane expression of ROMK to increase in the DCT2 and CNT (42) but do not easily translate into an understanding of how KS-WNK1 physiologically regulates ROMK. However, recent patch-clamp studies in mice demonstrated that KS-WNK1 is necessary for the physiological stimulation of

ROMK currents in response to a dietary potassium load (49), a condition known to stimulate KS-WNK1 transcription (40). We speculate that KS-WNK1 may affect ROMK differently depending on the circumstance and where it is expressed. In *Wnk1*$^{+/delE631}$ mice and patients, overexpressed KS-WNK1 in the DCT may indirectly inhibit ROMK in the CNT through distal nephron remodelling processes, as have been observed in a DCT-specific mouse model of FFHt (45). But when KS-WNK1 is physiologically activated in the CNT, its direct positive effects on ROMK would be completely opposite. Obviously, a test of these ideas will require further studies, perhaps with nephron-specific KS-WNK1 knockout and overexpression models.

The absence of hypertension in the patients and *Wnk1*$^{+/delE631}$ mice is puzzling given the increase in NCC phosphorylation. In that regard, it was interesting to compare the phenotypes of our FHHt patients depending on the *WNK1* or *WNK4* gene affected with similar genetic variants at the acidic motif of the kinase. Despite a relatively small number of affected subjects and difference in the median age of the two groups (39.5 vs 23.0 years), it was clear that WNK4 patients had a much higher blood pressure than those with similar mutations at the *WNK1* gene (median 163/102 mmHg vs 111/75 mmHg, respectively). In contrast, these two groups had a similar biological profile characterized by a marked hyperkalemia, hyperchloremia and metabolic acidosis. In addition, the *Wnk1*$^{+/delE631}$ mice are normotensive, even on a high sodium chloride diet. Only homozygous mice display a higher basal systolic BP (Supplemental Table 5). These *in vivo* observations highly suggest a differential effect on NaCl reabsorption between the two genes, independent of NCC stimulation. Interestingly, renin secretion was low in the patients with *WNK1* mutations at the acidic motif and renin transcription was reduced in *Wnk1*$^{+/delE631}$ mice, as expected from the negative feed-back loop of increased intravascular volume. However, ENaC expression was unchanged and natriuresis sensitivity to acute amiloride was not affected in mutant mice, suggesting that the hypertensive phenotype in FHHt may require increase ENaC activity. Finally, BP remained lower in *Wnk1*$^{+/delE631}$ mice fed a low K^+ diet compared to wild-type littermates, demonstrating that the hyperkalemia was not responsible for the renin inhibition. Taken together, these results suggest that *Wnk1*$^{+/delE631}$ mice and the patients display a mild hypervolemic state and that the full understanding of the mechanisms underlying the absence of hypertension remain to be identified.

In conclusion, the discovery of mutations within the WNK1 acidic motif and their *in vitro* and *in vivo* characterization uncover new features of the KS-WNK1 isoform. We found that KS-WNK1 acts as a positive modulator of NCC that is preferentially degraded at the protein level by the KLHL3-CUL3 ubiquitin complex compared with the L-WNK1 isoform. In the pathological conditions observed here, mutations in the acidic motif prevent KLHL3-CUL3 interaction, leading to an increased KS-WNK1 abundance, aberrant activation of NCC, and hyperkalemia without hypertension.

METHODS

HUMAN GENETIC STUDIES

Linkage analysis

Linkage in Ped29 was analyzed using markers generated by the 250K Affymetrix array *(Affymetrix, Inc.)*, as previously performed (38). We excluded non-polymorphic and low-frequency (minor allele frequency (MAF) < 0.1) SNPs. To decrease the SNPs list to a manageable set of 49,187 SNPs for linkage analysis, we applied a filter using the Bayesian Robust Linear Model with Mahalanobis distance classifier (BRLMM) and have only analyzed SNPs with BRLMM = 0.15. We applied the 1 Mb to 1 centimorgan conversion before analysis as recommended (50). Checks for Mendelian errors and parametric linkage analyzes were computed by MERLIN (51) under a rare dominant model with full penetrance (100%) and a disease allele frequency of 0.0005.

Sequencing

Whole exome sequencing

IntegraGen, Evry, France, performed library preparation, capture, sequencing, and variants detection and annotation. Exons of genomic DNA samples were captured using Agilent in-solution enrichment methodology with their biotinylated oligonucleotides probes library, followed by paired-end 75 bp massively parallel sequencing on Illumina HiSeq 2000 (see (52) for detailed explanations of the process). The bioinfomatics analysis of deep sequencing data was based on the Illumina pipeline (CASAVA 1.8).

Direct Sanger Sequencing

PCR amplification and Sanger sequencing from genomic DNA was performed using standard methods. The sequencing of the WNK1 ex7 and 25 was performed using the primers listed in Supplemental Table 7A.

IN VITRO FUNCTIONAL CHARACTERIZATION

Mutant proteins in Xenopus laevis oocytes

Vectors used for expressions in Xenopus oocytes and HEK293 cells are described in supplemental material. cRNA for Xenopus oocyte injections were prepared by in vitro transcription of the corresponding human clones after plasmid linearization using the T7 RNA polymerase m MESSAGE kit (Ambion).

We used *Xenopus laevis* oocytes as an expression system, approved and performed following the guidelines set by the Institutional Animal Care Committee of our institution. Oocytes preparation protocol has been described before (53). In brief, oocytes were obtained from female frogs under anesthesia and the follicular layer was removed. After 24 hours oocytes were injected with 50 nl of H_2O alone or containing 0.2 µg/µl of each clone cRNA. After 48 hours of incubation protein extracts were obtained using lysis buffer containing 50 mM Tris· HCl (pH 7.5), 1 mM EGTA, 1 mM EDTA, 50 mM sodium fluoride, 5 mM sodium pyro-phosphate, 1 mM sodium orthovanadate, 1% (wt/vol) Nonidet P-40, 0.27 M sucrose, 0.1% (vol/vol) 2-mercaptoethanol, and protease inhibitors (Complete tablets; Roche). Protein extracts equivalent to one oocyte (60 μ g) were resolved using SDS/PAGE and transferred to PVDF membranes for western blot analysis. The antibodies used were commercial c-myc (11814150001, Roche/sigma) and flag antibody (M2, A6592; Sigma) at 1:1000 and 1:5000, as well as commercial anti beta-actin (sc47778; Santa-Cruz Biotechnology) at 1:2500. Immobilized antigens were detected by chemiluminesence using the Luminata Forte Western HRP substrate (Merck Millipore)

Mutant proteins in HEK293T cells

Cell culture and transfection

Flp-InTM T-RExTM 293 cells (Invitrogen) were stably transfected with pCDNA5/FRT/(His)6-Protein C-Flag-hKLHL3 WT or R528H vector following the manufacturer's instructions. Conditions of culture and induction are described in supplemental material. For expression of WNK1-myc constructs (pcDNA vectors described in supplemental material) and Ubiquitin-HA, cells were transiently transfected using Effectene® (Qiagen) following the manufacturer's instructions.

Immunoprecipitation

Cells were harvested 48h post-transfection, washed in cold PBS and frozen in liquid nitrogen.
Lysis/immunoprecipitation of cell pellets in denaturing or native conditions were performed according to classical procedures described in supplemental material.

Immunoblotting

Lysates and immunoprecipitates were analyzed by SDS-PAGE (6% or 8% gels), transferred to nitrocellulose membrane, and immunoblotted with primary antibodies including anti-HA (Cell Signalling), anti-myc (9B11, Cell Signalling), anti-protein C (hpc4, Roche), rabbit anti-GAPDH (ab37168; Abcam), goat anti-actin (sc47778; Santa-Cruz). Thereafter, the membranes were incubated with a horseradish peroxidase-conjugated secondary antibody (1:5000 dilution). The images were obtained with chemiluminescence (Pierce ECL Western Blotting Substrate**)** using a luminescent image analyzer (LAS-4000 mini, Fujifilm) and quantified with MultiGauge software.

MOUSE EXPERIMENTAL STUDIES

Crispr/Cas9 engineered mice

In order to produce the c.1905T>A, p.D635E mutation at exon 7 of the mouse *Wnk1* gene using the CRISPR/Cas9 system, we have chosen three 20mers sgRNAs (in Supplemental Table 7C), using the CRISPR Design algorithm (http://tools.genome-engineering.org). SgRNAs were produced with Cas9 SmartNuclease™ RNA System (SBI Ozyme) and quality was controlled by Experion™ Automated Electrophoresis System (BioRad).

One cell zygotes (3 series of 100 oocytes) were co-injected with CAS9WT protein (New England Biolabs), one of the 3 sgRNA and a single strand 160mers nucleotide (ssODN) carrying the acidic motif mutation and 80 bases of flanking sequence on each side of the cut (54) (Supplemental Table 7C). This ssODNs has been designed to achieve high HDR efficiency, sgRNA/ CAS9 system efficiency was validated in vitro by PCR digestion.

About 10% of injected zygotes (30 blastocystes) were amplified by PCR (primers in Supplemental Table 7C) and analyzed by HRM, ddPCR (Biorad) and sequencing to identify indel or mutations. After birth, mice biopsies were analyzed by sequencing.

Radio-Telemetry Monitoring of Blood Pressure and Heart Rate

The study was performed on 14 C57Bl6J male mice divided in 2 subgroups (7 controls *Wnk1*$^{+/+}$, 7 *Wnk1*$^{+/delE631}$ mice). Mice were implanted with blood pressure and heart rate measuring telemetric probes (DSI, USA). The precise monitoring of the animals is described in supplemental methods.

Physiological and pharmacological challenges*Basal conditions* - Animals were housed in metabolic cages and fed a standard diet (0.3% NaCl) with free access to tap water. After a 3-day adaptation period, urines were collected daily for electrolyte measurements for 2 days.

Diets - The standard diet contained 0.3% NaCl and 1% KCl; low K diet contained 0.3% NaCl and 0% KCl; high salt diet contained 3% NaCl and 1% KCl;

Amiloride - After a 3 day-adaptation period, physiological saline was injected intra-peritoneally at 10:00 am and urine was collected 6 hours after the injection. The same procedure was repeated the day after with an injection of amiloride (1.45 mg/kg body weight), dissolved in physiological saline. For the analysis of the variations in physiological ROMK expression response to blood potassium increase as well as for the measurement of transtubular potassium gradient (TTKG), amiloride was administered intraperitoneally at the same dose during 4 days.

Hydrochlorothiazide (HCTZ) - Animals were fed with a specific diet supplemented with hydrochlorothiazide (HCTZ 240mg/kg/day oral) during 4-7 days such as done in previous studies (13, 19) for analysis of blood pressure response and analysis of the TTKG variations.

Metolazone – Metolazone (50µg/kg/day) was administered intraperitoneally during 4 days.

Blood and urine measurements

Plasma electrolytes were measured using an i-STAT® system (Abbott) and EC-8+ cartridges test. Blood samples were collected under Isofurane anesthesia by retroorbital puncture. Creatinine was determined using an Olympus AU400 analyser. Urinary aldosterone was measured by competitive chemiluminescent immunoassay (LIAISON® Aldosterone kit from Diasorin). Transtubular potassium gradient (TTKG) was calculated as follows (26): TTKG = ([K+] urine / [K+] blood) x (Osmblood / Osmurine) as have been used widely before in animal model studies to estimate the potassium secretory capacity of the distal nephron. Although urea recycling has been argued to make TTKG greater than the actual value in vivo (55), the error is small (~10%) because it the urea reabsorption is offset by passive potassium reabsorption in the inner medullary collecting duct (56). This is in agreement with experimental measurements that have validated the TTKG calculation as a reasonable estimate of the potassium secretory capacity in rodents (57). Although we cannot rule out the urea recycling or passive potassium reabsorption is affected by the WNK1 exon 7 mutation, it seems unlikely. Nevertheless, we acknowledge this as a limitation.

RNA Extraction and RT-qPCR for renin expression.

The extraction of total RNA from mouse kidneys, reverse transcription, and RT-qPCR were performed as described in (12). Primers sequences are indicated in Supplemental Table 7D:

Ubiquitin c (ubc) was used a reference gene, and comparative quantification of the gene of interest between the two genotypes was obtained using the $2^{-\Delta\Delta Ct}$ method.

Mouse kidney immunoblotting

At the end of the experimental period, animals were sacrificed with ketamine and xylazine (0.1 and 0.01 mg/g of body weight, respectively).

Renal cortex or total renal samples were homogenized, extracted and submitted to SDS/PAGE electrophoresis, and immunoblotting as detailed in supplemental methods.

.

WNK1 and ROMK1 Immunolocalization in the cortical nephron

WNK1 and ROMK1 immunofluorescence experiments were performed on kidneys embedded in paraffin. All technical details are given in supplemental methods.

Statistics overview

Human studies : data were analyzed using Fisher exact and t-tests. All tests were two-sided. P values < 0.05 were considered significant.

Mouse studies : when analysing two groups of mice, we used an unpaired student t-test. An one-way ANOVA followed by Sidak's multiple comparisons test was used to analyze more than two groups with $n \geq 5$ while a Kruskal-Wallis followed by a Mann-Whitney test was used to analyze more than two groups with $n < 5$. Data are given as mean ± s.e.m. A difference between groups was considered significant when $P < 0.05$.

Study approval

Study subjects. Affected individuals were recruited at the Department of Genetics of the Hôpital Européen Georges Pompidou as well as at other Departments of Nephrology located in France, Italy and UK. Genetic testing and research was performed according to the French ethic law published in 2001 (articles L.1110-4 al 1 CSP and R 1131-14 CSP). Informed written consent was obtained from all study participants. The study and corresponding database were approved by the local ethical committee : "Assistance Publique Hôpitaux de Paris, Comité de Protection des Personnes, Paris-Île de France XI (# 09069), Paris, France"

Mouse experiments. All studies were conducted on 3- to 5-month-old male mice and performed in accordance with the European Communities Council Directive. The project has been approved by the French Ministry of Research (#02650.02).

ACKNOWLEDGEMENTS

We thank all patients and families for their participation to the study. We acknowledge the contributions of additional clinicians for the clinical and biochemical characterization of FHHt patients, especially Dr Béatrice Fiquet and Geneviève Beaurain (Paris, France), Dr Patrick Giraud (Montauban, France), Dr Silvia Monticone (Torino, Italy). We also thank Valérie Boccio for her contribution to the genetic analysis of the *WNK1* gene.

FUNDING

This work was supported by the Institut National de la Santé et de la Recherche Médicale (Inserm), the Fondation pour la Recherche pour l'Hypertension Artérielle (XJ and JH), the Transatlantic Network on Hypertension funded by the Fondation Leducq to XJ, GG, JH and OS; the Transatlantic Network on Potassium and Hypertension funded by the Fondation Leducq to PW and OS; by Agence Nationale pour la Recherche (ANR) (Grant JH, GB). This study received also funding from the European Union's Seventh Framework Programme (FP7/2007-2013) under grant agreement no. 305608 (EURenOmics). IK was supported by a grant from Institut de Recherche Servier and PM is supported by a grant from MIUR (ex-60% 2016 and 2017). This study was also supported by grants No. 23 from the "Fronteras de la Ciencia" of the Mexican Council of Science and Technology, and No. IN207716 from PAPIIT-DGAPA to GG; a collaborative funding from CONACYT - Agence Nationale pour la Recherche (Conacyt 188712-ANR-12-ISVS1-0001-01) to GG and JH.

O.S and S.V. were supported by the Swiss National Science Foundation Grant 310030-141013 and the NCCR-Kidney.ch (Swiss National Science Foundation). PW was supported by grants from the NIH (DK054231 and DK093501).

DISCLOSURE

The authors declare no competing financial interests. RU is Emeritus Professor of Nephrology at UCL and is currently working in Early Clinical Development, Early CVRM (Cardiovascular, Renal and Metabolism), R&D BioPharmaceuticals, AstraZeneca, Cambridge, UK and Gothenburg, Sweden

AUTHOR CONTRIBUTIONS

H.LDP. and N.T. conducted the human genetic studies, I.K., W.A-K., C.R., T.F. and M.C.C. performed the in vitro cellular experiments from mouse models, E.R.A., S.V., O.S. and G.G. performed the Xenopus oocytes studies, R.C., R.G. and P.A.W. performed the ROMK1 experiments, I.L-F., M.D.C., S.B., T.M., C.F. and J.H. conducted in vivo experiments from mouse studies, M.H., S.D., X.G., K.O., P.M., G.R., I.T., R.U. and R.V-P. acquired and analyzed clinical human data, P.W., G.G, E.C., J.H., and X.J. designed the research studies, assembled the figures and tables and wrote the manuscript, X.J. coordinated the entire study.

Correspondence and requests for materials should be addressed to X.J. (xavier.jeunemaitre@inserm.fr)**.**

REFERENCES

1. **Gordon RD, Klemm, S. A., Tunny, T.J. et al. In: Brenner JHLaBM ed. *Hypertension: Pathology, Diagnosis and Management*. New York: Raven Press Ltd; 1995:2111-3.**

2. **Wilson FH, Disse-Nicodeme S, Choate KA, Ishikawa K, Nelson-Williams C, Desitter I, et al. Human hypertension caused by mutations in WNK kinases. *Science.* 2001;293(5532):1107-12.**

3. **Boyden LM, Choi M, Choate KA, Nelson-Williams CJ, Farhi A, Toka HR, et al. Mutations in kelch-like 3 and cullin 3 cause hypertension and electrolyte abnormalities. *Nature.* 2012;482(7383):98-102.**

4. **Louis-Dit-Picard H, Hadchouel J, and Jeunemaitre X. [KLHL3 and CULLIN-3: new genes involved in familial hypertension]. *Med Sci (Paris).* 2012;28(8-9):703-6.**

5. **Ohta A, Schumacher FR, Mehellou Y, Johnson C, Knebel A, Macartney TJ, et al. The CUL3-KLHL3 E3 ligase complex mutated in Gordon's hypertension syndrome interacts with and ubiquitylates WNK isoforms: disease-causing mutations in KLHL3 and WNK4 disrupt interaction. *Biochem J.* 2013;451(1):111-22.**

6. **Shibata S, Zhang J, Puthumana J, Stone KL, and Lifton RP. Kelch-like 3 and Cullin 3 regulate electrolyte homeostasis via ubiquitination and degradation of WNK4. *Proc Natl Acad Sci U S A.* 2013;110(19):7838-43.**

7. **Wakabayashi M, Mori T, Isobe K, Sohara E, Susa K, Araki Y, et al. Impaired KLHL3-mediated ubiquitination of WNK4 causes human hypertension. *Cell Rep.* 2013;3(3):858-68.**

8. **Wu G, and Peng JB. Disease-causing mutations in KLHL3 impair its effect on WNK4 degradation. *FEBS Lett.* 2013;587(12):1717-22.**

9. **Achard JM, Disse-Nicodeme S, Fiquet-Kempf B, and Jeunemaitre X. Phenotypic and genetic heterogeneity of familial hyperkalaemic hypertension (Gordon syndrome). *Clin Exp Pharmacol Physiol.* 2001;28(12):1048-52.**

10. **Hadchouel J, Delaloy C, Faure S, Achard JM, and Jeunemaitre X. Familial hyperkalemic hypertension. *J Am Soc Nephrol.* 2006;17(1):208-17.**

11. **Delaloy C, Lu J, Houot AM, Disse-Nicodeme S, Gasc JM, Corvol P, et al. Multiple promoters in the WNK1 gene: one controls expression of a kidney-specific kinase-defective isoform. *Mol Cell Biol.* 2003;23(24):9208-21.**

12. **Vidal-Petiot E, Cheval L, Faugeroux J, Malard T, Doucet A, Jeunemaitre X, et al. A new methodology for quantification of alternatively spliced exons reveals a highly tissue-specific expression pattern of WNK1 isoforms. *PLoS One.* 2012;7(5):e37751.**

13. **Vidal-Petiot E, Elvira-Matelot E, Mutig K, Soukaseum C, Baudrie V, Wu S, et al. WNK1-related Familial Hyperkalemic Hypertension results from an increased expression of L-WNK1 specifically in the distal nephron. *Proc Natl Acad Sci U S A.* 2013;110(35):14366-71.**

14. **Schumacher FR, Sorrell FJ, Alessi DR, Bullock AN, and Kurz T. Structural and biochemical characterization of the KLHL3-WNK kinase interaction important in blood pressure regulation. *Biochem J.* 2014;460(2):237-46.**

15. **Wuermser LA, Reilly C, Poindexter JR, Sakhaee K, and Pak CY. Potassium-magnesium citrate versus potassium chloride in thiazide-induced hypokalemia. *Kidney Int.* 2000;57(2):607-12.**

16. **Matos V, van Melle G, Boulat O, Markert M, Bachmann C, and Guignard JP. Urinary phosphate/creatinine, calcium/creatinine, and magnesium/creatinine ratios in a healthy pediatric population. *J Pediatr.* 1997;131(2):252-7.**

17. **Sealey JE, Clark I, Bull MB, and Laragh JH. Potassium balance and the control of renin secretion. *J Clin Invest.* 1970;49(11):2119-27.**

18. **Yang SS, Morimoto T, Rai T, Chiga M, Sohara E, Ohno M, et al. Molecular pathogenesis of pseudohypoaldosteronism type II: generation and analysis of a Wnk4(D561A/+) knockin mouse model. *Cell Metab.* 2007;5(5):331-44.**

19. **Lalioti MD, Zhang J, Volkman HM, Kahle KT, Hoffmann KE, Toka HR, et al. Wnk4 controls blood pressure and potassium homeostasis via regulation of mass and activity of the distal convoluted tubule. *Nat Genet.* 2006;38(10):1124-32.**

20. **Rafiqi FH, Zuber AM, Glover M, Richardson C, Fleming S, Jovanovic S, et al. Role of the WNK-activated SPAK kinase in regulating blood pressure. *EMBO Mol Med.* 2010;2(2):63-75.**

21. **Yang SS, Lo YF, Wu CC, Lin SW, Yeh CJ, Chu P, et al. SPAK-knockout mice manifest Gitelman syndrome and impaired vasoconstriction. *J Am Soc Nephrol.* 2010;21(11):1868-77.**

22. **McCormick JA, and Ellison DH. The WNKs: atypical protein kinases with pleiotropic actions. *Physiol Rev.* 2011;91(1):177-219.**

23. **Rafael C, Soukaseum C, Baudrie V, Frere P, and Hadchouel J. Consequences of SPAK inactivation on Hyperkalemic Hypertension caused by WNK1 mutations: evidence for differential roles of WNK1 and WNK4. *Sci Rep.* 2018;8(1):3249.**

24. **Boyd-Shiwarski CR, Shiwarski DJ, Roy A, Namboodiri HN, Nkashama LJ, Xie J, et al. Potassium-regulated distal tubule WNK bodies are kidney-specific WNK1 dependent. *Mol Biol Cell.* 2018;29(4):499-509.**

25. **Thomson MN, Schneider W, Mutig K, Ellison DH, Kettritz R, and Bachmann S. Patients with hypokalemia develop WNK bodies in the distal convoluted tubule of the kidney. *Am J Physiol Renal Physiol.* 2019;316(2):F292-F300.**

26. **Choi MJ, and Ziyadeh FN. The utility of the transtubular potassium gradient in the evaluation of hyperkalemia. *J Am Soc Nephrol.* 2008;19(3):424-6.**

27. **Richardson C, Sakamoto K, de los Heros P, Deak M, Campbell DG, Prescott AR, et al. Regulation of the NKCC2 ion cotransporter by SPAK-OSR1-dependent and -independent pathways. *J Cell Sci.* 2011;124(Pt 5):789-800.**

28. **Hughey RP, Mueller GM, Bruns JB, Kinlough CL, Poland PA, Harkleroad KL, et al. Maturation of the epithelial Na+ channel involves proteolytic processing of the alpha- and gamma-subunits. *J Biol Chem.* 2003;278(39):37073-82.**

29. **Masilamani S, Kim GH, Mitchell C, Wade JB, and Knepper MA. Aldosterone-mediated regulation of ENaC alpha, beta, and gamma subunit proteins in rat kidney. *J Clin Invest.* 1999;104(7):R19-23.**

30. **Wade JB, Fang L, Liu J, Li D, Yang CL, Subramanya AR, et al. WNK1 kinase isoform switch regulates renal potassium excretion. *Proc Natl Acad Sci U S A.* 2006;103(22):8558-63.**

31. **Liu Z, Xie J, Wu T, Truong T, Auchus RJ, and Huang CL. Downregulation of NCC and NKCC2 cotransporters by kidney-specific WNK1 revealed by gene disruption and transgenic mouse models. *Hum Mol Genet.* 2011;20(5):855-66.**

32. **Castrop H, and Schiessl IM. Physiology and pathophysiology of the renal Na-K-2Cl cotransporter (NKCC2).** ***Am J Physiol Renal Physiol.*** **2014;307(9):F991-F1002.**

33. **Cheng CJ, Truong T, Baum M, and Huang CL. Kidney-specific WNK1 inhibits sodium reabsorption in the cortical thick ascending limb.** ***Am J Physiol Renal Physiol.*** **2012;303(5):F667-73.**

34. **Margolis BL, and Lifschitz MD. The Spitzer-Weinstein syndrome: one form of type IV renal tubular acidosis and its response to hydrochlorothiazide.** ***Am J Kidney Dis.*** **1986;7(3):241-4.**

35. **Spitzer A, Edelmann CM, Jr., Goldberg LD, and Henneman PH. Short stature, hyperkalemia and acidosis: A defect in renal transport of potassium.** ***Kidney Int.*** **1973;3(4):251-7.**

36. **Weng CH, Cheng JW, Hung CC, Wu MS, Yang CW, and Chang CT. A young female with Spitzer-Weinstein syndrome diagnosed by thiazide test.** ***Ren Fail.*** **2007;29(2):239-41.**

37. **Uchida S, Chiga M, Sohara E, Rai T, and Sasaki S. Does a beta2-adrenergic receptor-WNK4-Na-Cl co-transporter signal cascade exist in the in vivo kidney?** ***Nat Med.*** **2012;18(9):1324-5; author reply 1325-7.**

38. **Louis-Dit-Picard H, Barc J, Trujillano D, Miserey-Lenkei S, Bouatia-Naji N, Pylypenko O, et al. KLHL3 mutations cause familial hyperkalemic hypertension by impairing ion transport in the distal nephron.** ***Nat Genet.*** **2012;44(4):456-60, S1-3.**

39. **Piala AT, Moon TM, Akella R, He H, Cobb MH, and Goldsmith EJ. Chloride sensing by WNK1 involves inhibition of autophosphorylation.** ***Sci Signal.*** **2014;7(324):ra41.**

40. **O'Reilly M, Marshall E, Macgillivray T, Mittal M, Xue W, Kenyon CJ, et al. Dietary electrolyte-driven responses in the renal WNK kinase pathway in vivo.** ***J Am Soc Nephrol.*** **2006;17(9):2402-13.**

41. **Thomson MN, Cuevas CA, Bewarder TM, Dittmayer C, Miller LN, Si J, et al. WNK bodies cluster WNK4 and SPAK/OSR1 to promote NCC activation in hypokalemia.** ***Am J Physiol Renal Physiol.*** **2020;318(1):F216-F28.**

42. **Hadchouel J, Soukaseum C, Busst C, Zhou XO, Baudrie V, Zurrer T, et al. Decreased ENaC expression compensates the increased NCC activity following inactivation of the kidney-specific isoform of WNK1 and prevents hypertension.** ***Proc Natl Acad Sci U S A.*** **2010;107(42):18109-14.**

43. **Sasaki E, Susa K, Mori T, Isobe K, Araki Y, Inoue Y, et al. KLHL3 Knockout Mice Reveal the Physiological Role of KLHL3 and the Pathophysiology of Pseudohypoaldosteronism Type II Caused by Mutant KLHL3.** ***Mol Cell Biol.*** **2017;37(7):e00508-16.**

44. **Susa K, Sohara E, Rai T, Zeniya M, Mori Y, Mori T, et al. Impaired degradation of WNK1 and WNK4 kinases causes PHAII in mutant KLHL3 knock-in mice.** ***Hum Mol Genet.*** **2014;23(19):5052-60.**

45. **Grimm PR, Coleman R, Delpire E, and Welling PA. Constitutively Active SPAK Causes Hyperkalemia by Activating NCC and Remodeling Distal Tubules.** ***J Am Soc Nephrol.*** **2017;28(9):2597-606.**

46. **Subramanya AR, Yang CL, Zhu X, and Ellison DH. Dominant-negative regulation of WNK1 by its kidney-specific kinase-defective isoform.** ***Am J Physiol Renal Physiol.*** **2006;290(3):F619-24.**

47. **Chavez-Canales M, Zhang C, Soukaseum C, Moreno E, Pacheco-Alvarez D, Vidal-Petiot E, et al. WNK-SPAK-NCC cascade revisited: WNK1 stimulates the activity of the Na-Cl cotransporter via SPAK, an effect antagonized by WNK4.** ***Hypertension.*** **2014;64(5):1047-53.**

48. **Argaiz ER, Chavez-Canales M, Ostrosky-Frid M, Rodriguez-Gama A, Vazquez N, Gonzalez-Rodriguez X, et al. Kidney-specific WNK1 isoform (KS-WNK1) is a potent activator of WNK4 and NCC.** ***Am J Physiol Renal Physiol.*** **2018;315(3):F734-745**

49. **Wu P, Gao ZX, Su XT, Ellison DH, Hadchouel J, Teulon J, et al. Role of WNK4 and kidney-specific WNK1 in mediating the effect of high dietary K+ intake on ROMK channel in the distal convoluted tubule.** ***Am J Physiol Renal Physiol.*** **2018;315(2):F223-230**

50. **Ulgen A, and Li W. Comparing single-nucleotide polymorphism marker-based and microsatellite marker-based linkage analyses.** ***BMC Genet.*** **2005;6 Suppl 1:S13.**

51. **Abecasis GR, Cherny SS, Cookson WO, and Cardon LR. Merlin--rapid analysis of dense genetic maps using sparse gene flow trees.** ***Nat Genet.*** **2002;30(1):97-101.**

52. **Gnirke A, Melnikov A, Maguire J, Rogov P, LeProust EM, Brockman W, et al. Solution hybrid selection with ultra-long oligonucleotides for massively parallel targeted sequencing.** ***Nat Biotechnol.*** **2009;27(2):182-9.**

53. **Monroy A, Plata C, Hebert SC, and Gamba G. Characterization of the thiazide-sensitive Na(+)-Cl(-) cotransporter: a new model for ions and diuretics interaction.** ***Am J Physiol Renal Physiol.*** **2000;279(1):F161-9.**

54. **Chen F, Pruett-Miller SM, Huang Y, Gjoka M, Duda K, Taunton J, et al. High-frequency genome editing using ssDNA oligonucleotides with zinc-finger nucleases.** ***Nat Methods.*** **2011;8(9):753-5.**

55. **Kamel KS, and Halperin ML. Intrarenal urea recycling leads to a higher rate of renal excretion of potassium: an hypothesis with clinical implications.** ***Curr Opin Nephrol Hypertens.*** **2011;20(5):547-54.**

56. **Wen D, Cornelius RJ, Rivero-Hernandez D, Yuan Y, Li H, Weinstein AM, et al. Relation between BK-alpha/beta4-mediated potassium secretion and ENaC-mediated sodium reabsorption.** ***Kidney Int.*** **2014;86(1):139-45.**

57. **West ML, Bendz O, Chen CB, Singer GG, Richardson RM, Sonnenberg H, et al. Development of a test to evaluate the transtubular potassium concentration gradient in the cortical collecting duct in vivo.** ***Miner Electrolyte Metab.*** **1986;12(4):226-33.**

58. **Mayan H, Munter G, Shaharabany M, Mouallem M, Pauzner R, Holtzman EJ, et al. Hypercalciuria in familial hyperkalemia and hypertension accompanies hyperkalemia and precedes hypertension: description of a large family with the Q565E WNK4 mutation.** ***J Clin Endocrinol Metab.*** **2004;89(8):4025-30.**

59. **Golbang AP, Murthy M, Hamad A, Liu CH, Cope G, Van't Hoff W, et al. A new kindred with pseudohypoaldosteronism type II and a novel mutation (564D>H) in the acidic motif of the WNK4 gene.** ***Hypertension.*** **2005;46(2):295-300.**

60. **Gong H, Tang Z, Yang Y, Sun L, Zhang W, Wang W, et al. A patient with pseudohypoaldosteronism type II caused by a novel mutation in WNK4 gene.** ***Endocrine.*** **2008;33(3):230-4.**

FIGURES

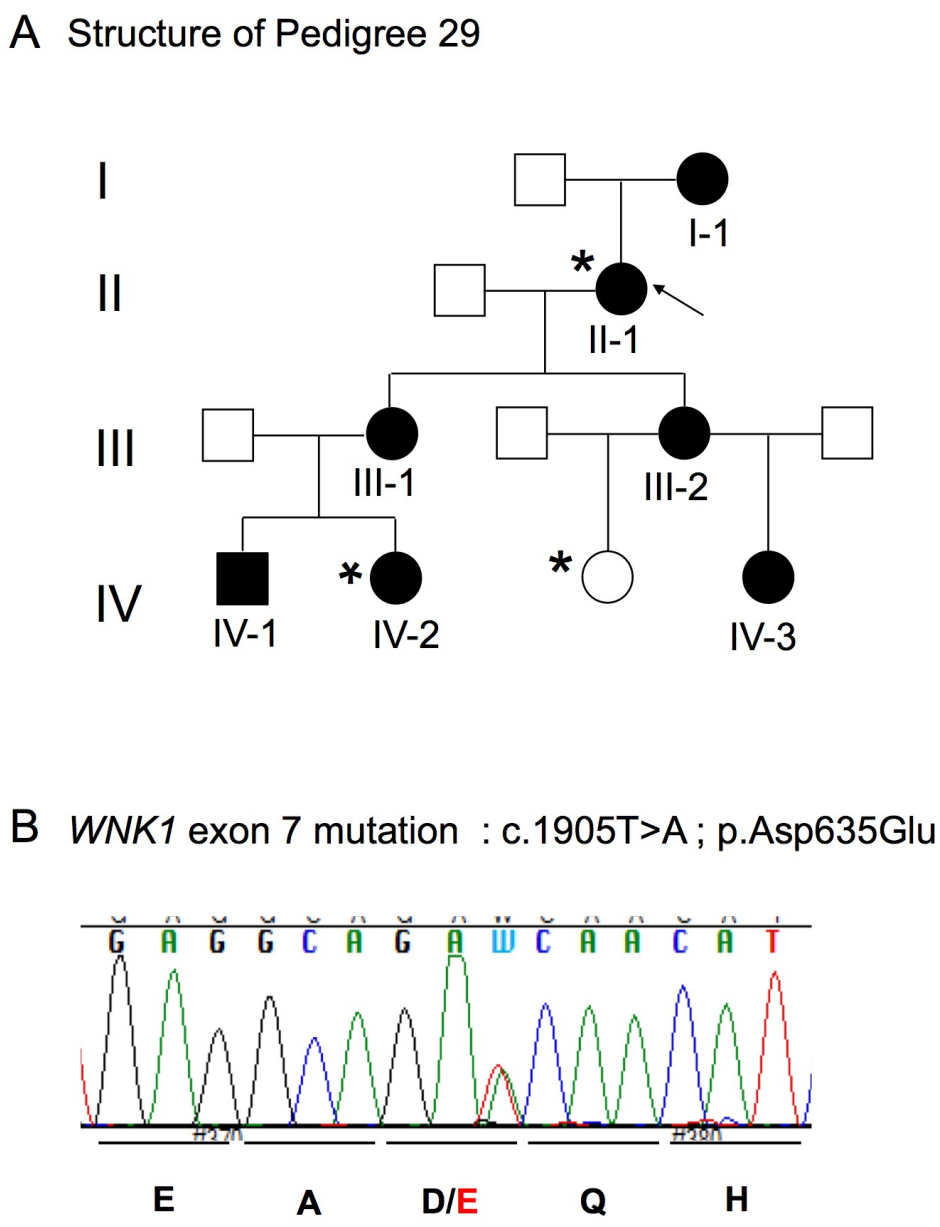

Figure 1: Missense variant in the *WNK1* acidic motif in the FHHt pedigree 29
A. Kindred 29: family affected by FHHt composed by 7 affected (black) and 6 unaffected (white) members. Arrow indicates the index case. Asterisks indicate exome sequenced individuals.
B. Electrophoregram obtained by Sanger sequencing showing the double peak A/T corresponding to the *WNK1* heterozygous mutation (c.1905T>A; p.Asp635Glu).

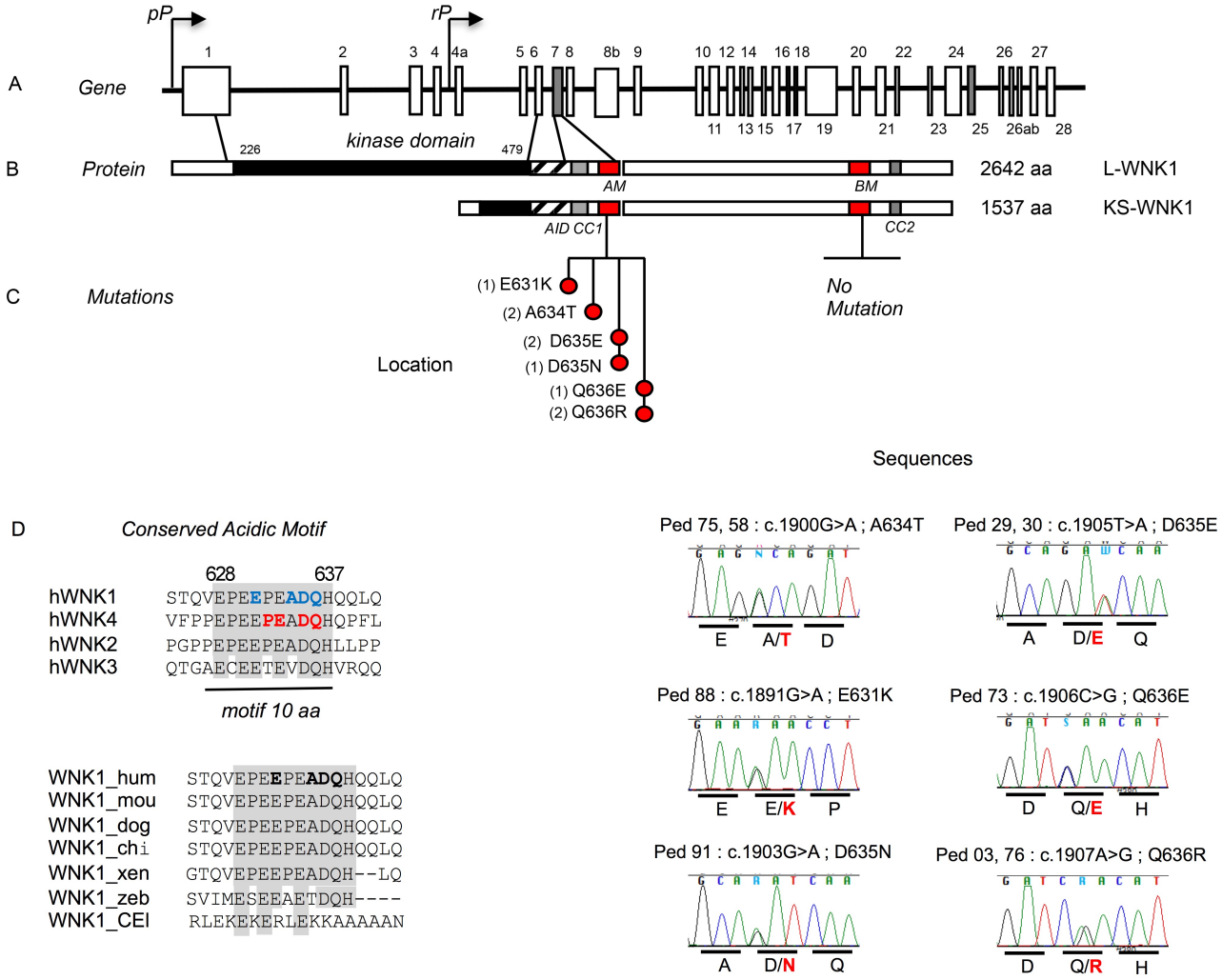

Figure 2: Acidic motif *WNK1* mutations

A. Schematic representation of the *WNK1* gene. The coordinates of the different exons are indicated above or below the structure with exons 7 and 25 in grey which code for the conserved acidic and basic motifs. The proximal promoter (pP) drives the expression of the long ubiquitous kinase active isoform (L-WNK1) whereas the renal promoter (rP) drives the expression of the kinase defective kidney-specific isoform (KS-WNK1)

B. Schematic linear structure of LWNK1 and KS-WNK1. The kinase domain is represented in full black, the auto-inhibitory domain (AID) is stripy, the coiled-coil domain 1 (CC1) and 2 (CC2) are represented in grey and the conserved acidic motif (AM) and basic motif (BM) are represented in red.

C. Location and sequences of the mutated residues clustering in the acidic motif. The brackets indicate the number of unrelated affected subjects for each mutation. On the right are shown the Sanger sequencing electrophoregrams showing the various missense *WNK1* mutations.

D. Conservation of the acidic motif showing residues mutated in FHHt among human WNK family members. The previously described *WNK4* mutations are indicated in red, those at *WNK1* and identified in this study in blue. All are located at completely conserved residues. The bottom part shows the conservation of the WNK1 acidic motif across species. The mutated residues are indicated in bold.

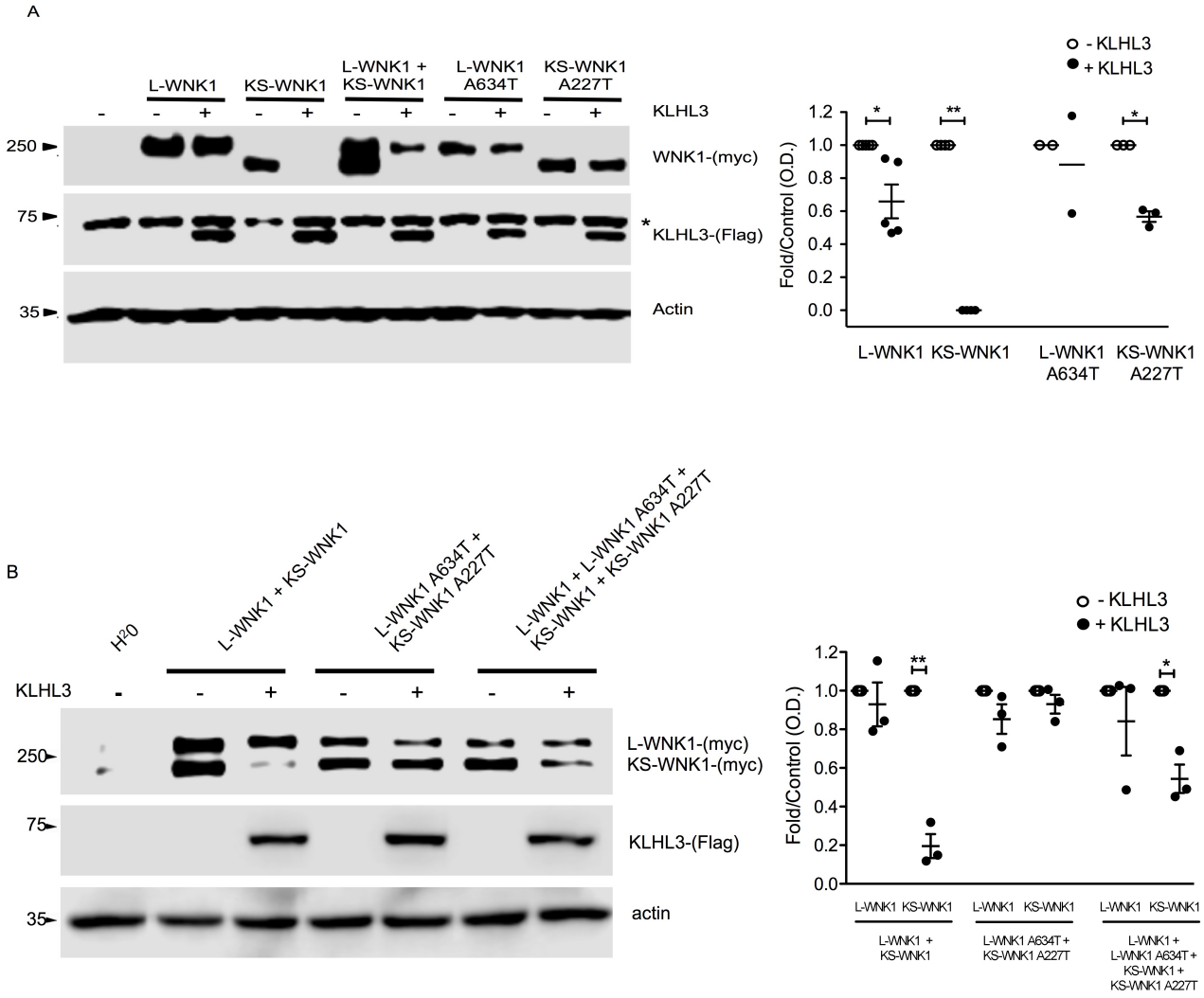

Figure 3: Differential effect of the WNK1 Ex7 G1900A (A634T-L-WNK1; A227T-KS-WNK1) variant on the interaction between KLHL3 and L-WNK1 or KS-WNK1 isoforms

A. Representative immunoblot of proteins extracted from *Xenopus laevis* oocytes (left panel) that were injected with wild type or mutant L-WNK1 or KS-WNK1 in the absence or presence of KLHL3 cRNA, as stated. The upper blot shows c-myc positive bands corresponding to L-WNK1 and KS-WNK1. The middle blot shows unspecific upper band present in all lanes (*), including water injected oocytes, and a lower band corresponding to KLHL3 only present in KLHL3 injected oocytes. The lower blot shows actin. Densitometry of several (n=3) blots in which the effect of KLHL3 was tested in L-WNK1 or KS-WNK1 wild type or mutants separately (right panel). In the absence of KLHL3, mean values were arbitrarily set to 1.0 and in the presence of KLHL3, values were normalized accordingly. *p<0.05, **p<0.01 (unpaired Student's t test).

B. Representative immunoblot of proteins extracted from *Xenopus laevis* oocytes (left panel) that were injected with mixture of wild type or mutant L-WNK1 and KS-WNK1 in the absence or presence of KLHL3 cRNA, in order to analyze the consequences of L-WNK1 and KS-WNK1 coexpression. Legends of the immunoblot (left panel) and densitometry analysis of several blots (right panel) are as in Figure 3A. *p<0.05, **p<0.01 (unpaired Student's t test).

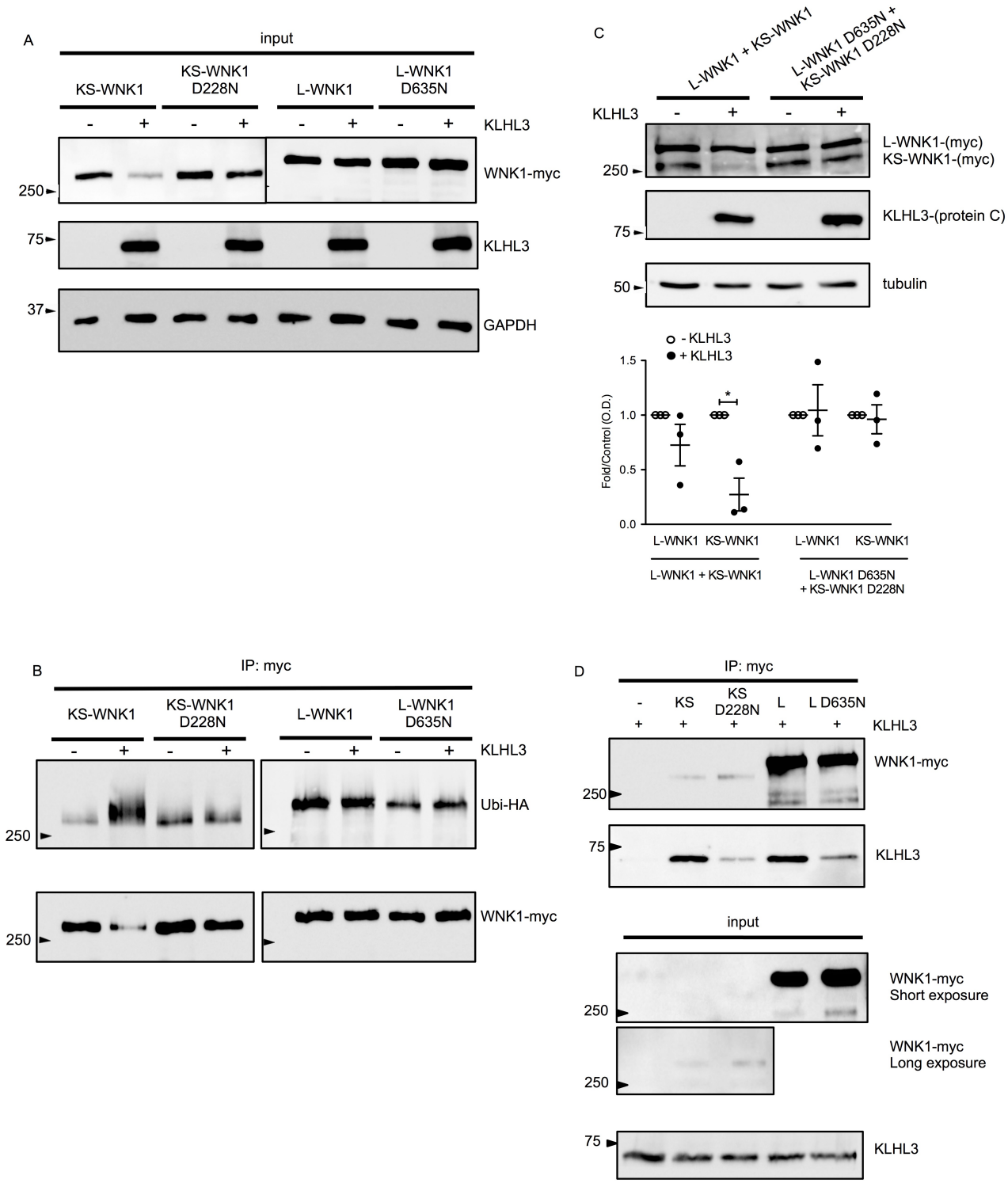

Figure 4 : KLHL3 interaction with WNK1 isoforms in HEK293T cells: KLHL3 ubiquitinates KS-WNK1 and significantly reduces its protein levels.

A. Flp-In T-Rex 293 cells stably and inducibly expressing (His)6-Protein C-Flag-hKLHL3 were transfected with myc-tagged L-WNK1 (wild-type or D635N mutant) or KS-WNK1 (wild-type or D228N mutant) , as indicated. 34 hours post-transfection cells were induced with tetracycline. 14 hours later (48h post-transfection) cells were harvested and lysed in denaturing conditions. Cell lysates were subjected to immunoblot analysis with the indicated antibodies. Data shown are representative of three independent experiments.

B. Flp-In T-Rex 293 cells stably and inducibly expressing (His)6-Protein C-Flag-hKLHL3 were transfected with ubiquitin-HA and myc-tagged L-WNK1, L-WNK1 D635N, KS-WNK1 or KS-WNK1 D228N, as indicated. 34 hours after transfection, cells were induced with tetracycline. 14 hours later (48h post-transfection), cells were harvested and lysed in denaturing conditions. Upper panel: Myc-tagged WNK1 isoforms were immunoprecipitated with anti-myc antibody (9B11, Cell Signaling); immunoprecipitates were analyzed by immunoblotting with anti-HA antibody (3724S Cell signalling). Nitrocellulose membranes were stripped and re-blotted with anti-myc antibody. Immunoblot of cell lysates is represented by Fig 4D (input). Data shown are representative of three independent experiments.
C. Cells were transfected with myc-tagged L-WNK1 (wild-type or D635N mutant) and KS-WNK1 (wild-type or D228N mutant), as indicated and in similar conditions as in Figure 4A. Cell lysates were subjected to immunoblot analysis with the indicated antibodies. Densitometric analysis was performed using the FUJI FILM Multi Gauge software. Results are shown as mean ±SEM. *$p<0,05$ compared with control. n=3. (unpaired Student's t test)
D. Flp-In T-Rex 293 cells stably and inducibly expressing (His)6-Protein C-Flag-hKLHL3 were transfected with myc-tagged L-WNK1, L-WNK1 D635N, KS-WNK1 or KS-WNK1 D228N, as indicated. 43h after transfection, cells were induced with tetracycline and simultaneously treated with MG132 for 5h. 48h post-transfection, cells were harvested and lysed in native conditions.
Upper panel: Cell lysates were immunoprecipitated with anti-myc antibody and immunoprecipitates were analyzed by immunoblotting with anti-protein C and anti-myc antibodies. Lower panel: Cell lysates (input) were subjected to immunoblot analysis with anti-myc and anti-protein C antibodies (HPC4, Roche) to check for even expression of KLHL3. Data shown are representative of three independent experiments.

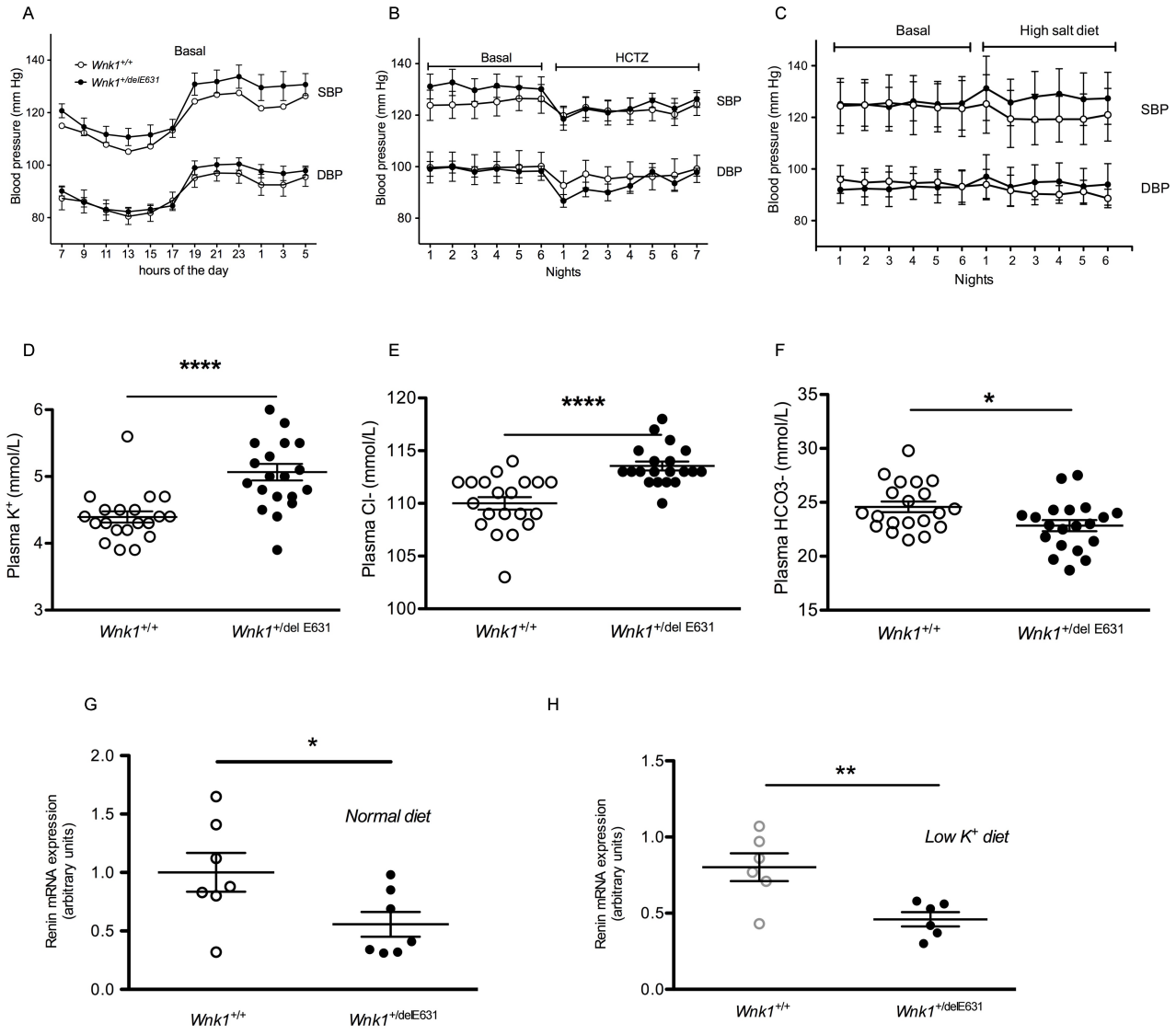

Figure 5: Normal blood pressure on both normal and high salt diet in *Wnk1*$^{+/delE631}$ mice

A-C. Systolic blood pressure (SBP) and diastolic blood pressure (DBP). SBP and DBP profiles over 24 h of systolic blood pressure (SBP) and diastolic blood pressure (DBP) under a 12:12-h day-night schedule in *Wnk1*$^{+/+}$ (n=6) and *Wnk1*$^{+/delE631}$ (n=7) mice instrumented with a telemetric system under basal condition (A). Night SBP and DBP of the same mice before (6 nights = basal) or during (7 nights) the oral administration of hydrochlorothiazide (HCTZ 240mg/kg/day) (B). Night SBP and DBP of another series mice (n=4 *Wnk1*$^{+/+}$, n=4 *Wnk1*$^{+/delE631}$) before (6 nights = basal) or during (6 nights) the administration of high (3%) Na+ diet (C).
D-F. Biological characteristics. In the mutant mice, significant hyperkalemia (5.1 ± 0.5 vs 4.3 ± 0.2, ****p<0.0001; n=20)(D); hyperchloremia (114 ± 2 vs 110 ± 3, ****p<0.0001; n=20) (E) and metabolic acidosis ($HCO3^-$ 22.8 ± 2.1 vs 24.6 ± 2.5, *p<0.05; n=20) (F) were observed together with normal creatinine values (not shown). Data are means ± SEM. Statistical comparisons were made using unpaired Student's t-test.
G-H. Renin expression. The level of renin mRNA was measured by RT-qPCR in the kidney cortex of *Wnk1*$^{+/+}$ (n=7) and *Wnk1*$^{+/delE631}$ (n=7) mice in baseline conditions (G) or of *Wnk1*$^{+/+}$ (n=6) and *Wnk1*$^{+/delE631}$ (n=6) mice fed a low (0%) K^+ diet (H). Results (mean ± SEM) are expressed in arbitrary units relative to the expression of ubc. The expression level in *Wnk1*$^{+/+}$ mice in basal conditions was arbitrarily set to one. *p< 0.05; **p< 0.01 (unpaired Student's t test).

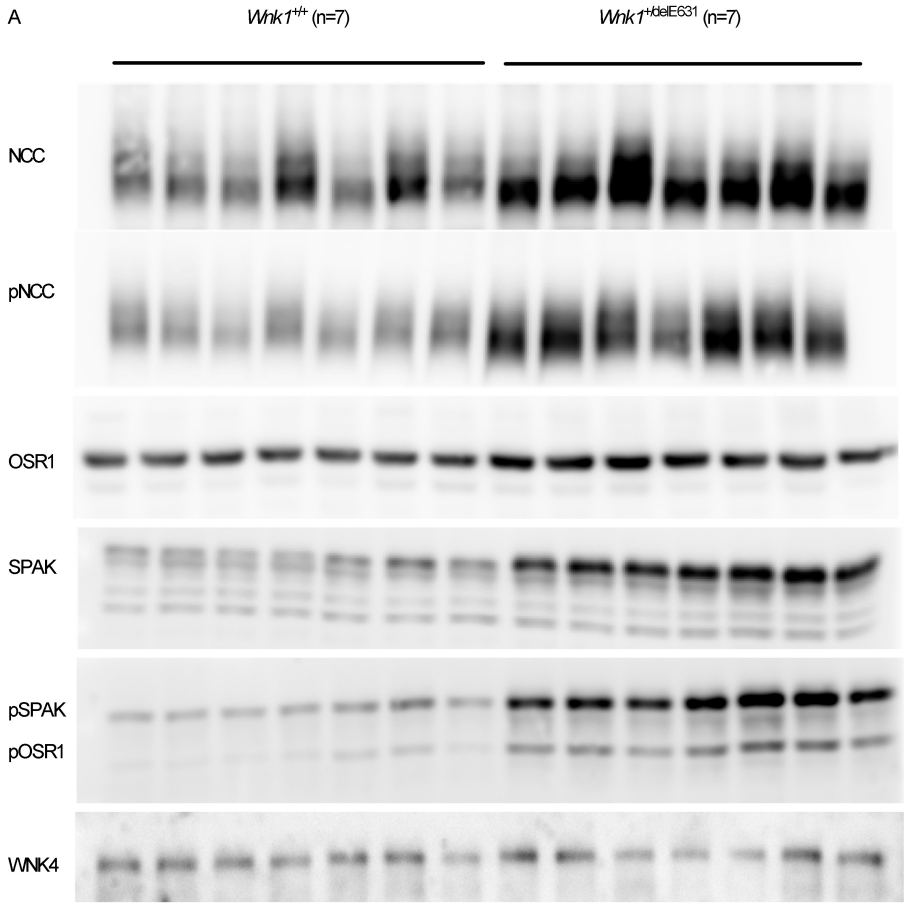

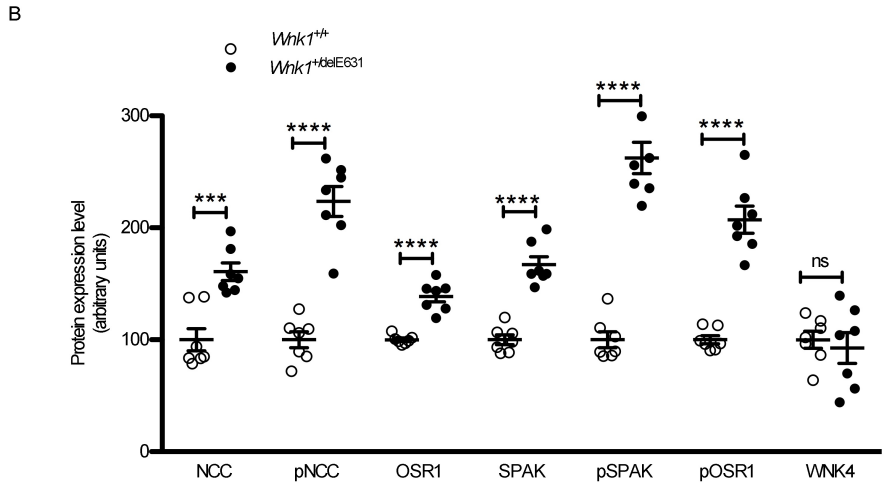

Figure 6: Activation of the SPAK-NCC phosphorylation cascade in *Wnk1*$^{+/delE631}$ mice.
A: Representative immunoblots with the indicated antibodies performed on the membrane-enriched fractions (NCC and pNCC) or total homogenates of the renal cortex of mice of each genotype.
B: Densitometric analysis. NCC, SPAK and OSR1 abundance and phosphorylation are increased in *Wnk1*$^{+/delE631}$ mice compared to *Wnk1*$^{+/+}$ mice. WNK4 expression is similar between the two groups of mice. The expression level in *Wnk1*$^{+/+}$ mice was arbitrarily set to 100. Values are means ± SEM. ***p<0.001, ****p<0.0001 (unpaired Student's t test).

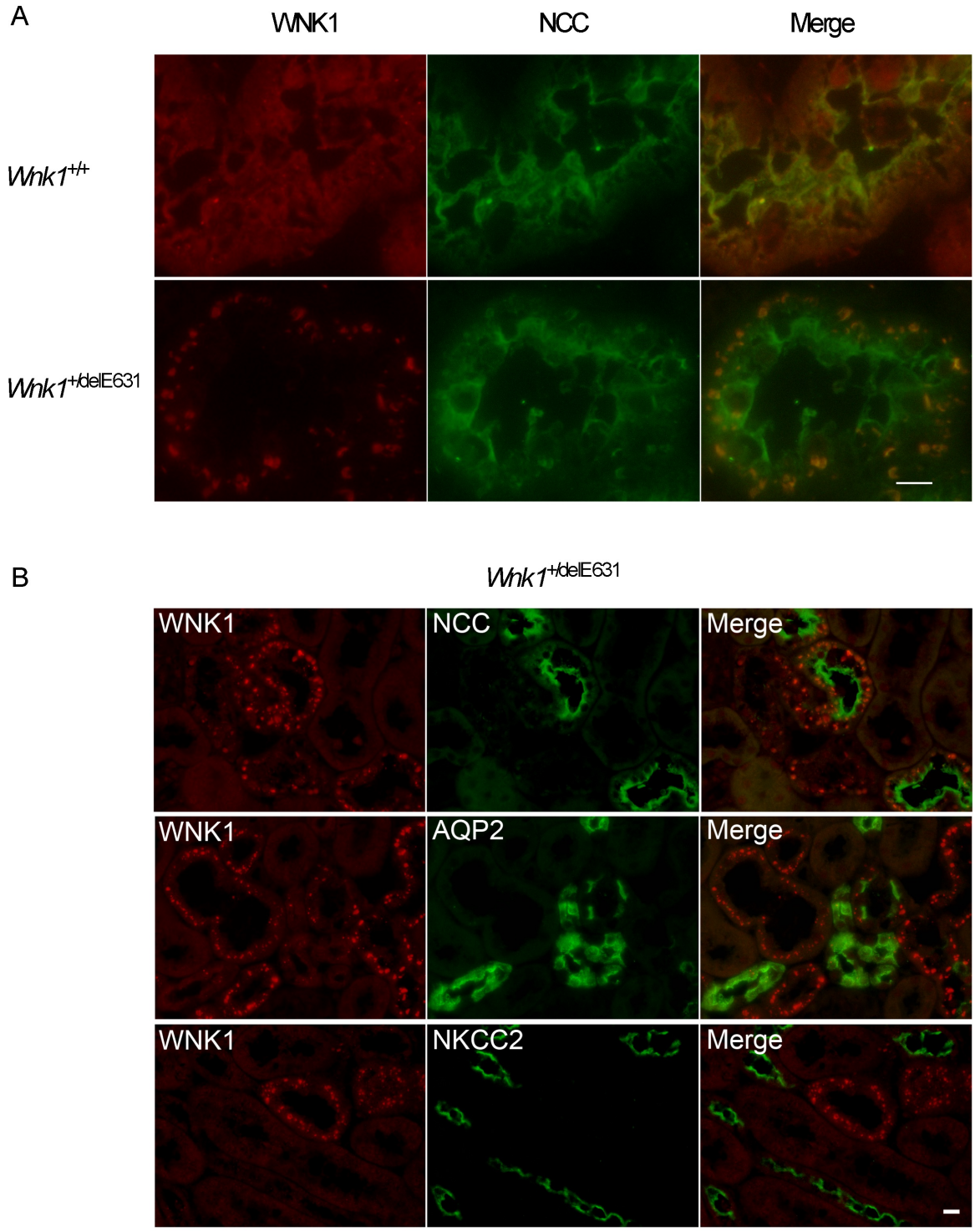

Figure 7: The DCTs of *Wnk1*$^{+/delE631}$ mice contain large WNK bodies.

(A) Immunofluorescence experiments using WNK1 and NCC antibodies. While only small puncta are observed in *Wnk1*$^{+/+}$ DCT, large WNK1-positive structures are found in *Wnk1*$^{+/delE631}$ DCT, resembling the previously described WNK bodies (scale bar 10µm).

(B) Co-staining with NCC, AQP2 and NKCC2 revealed that these bodies are localized in the DCT and CNT/CCD but not in Henle's loop (scale bar 20µm).

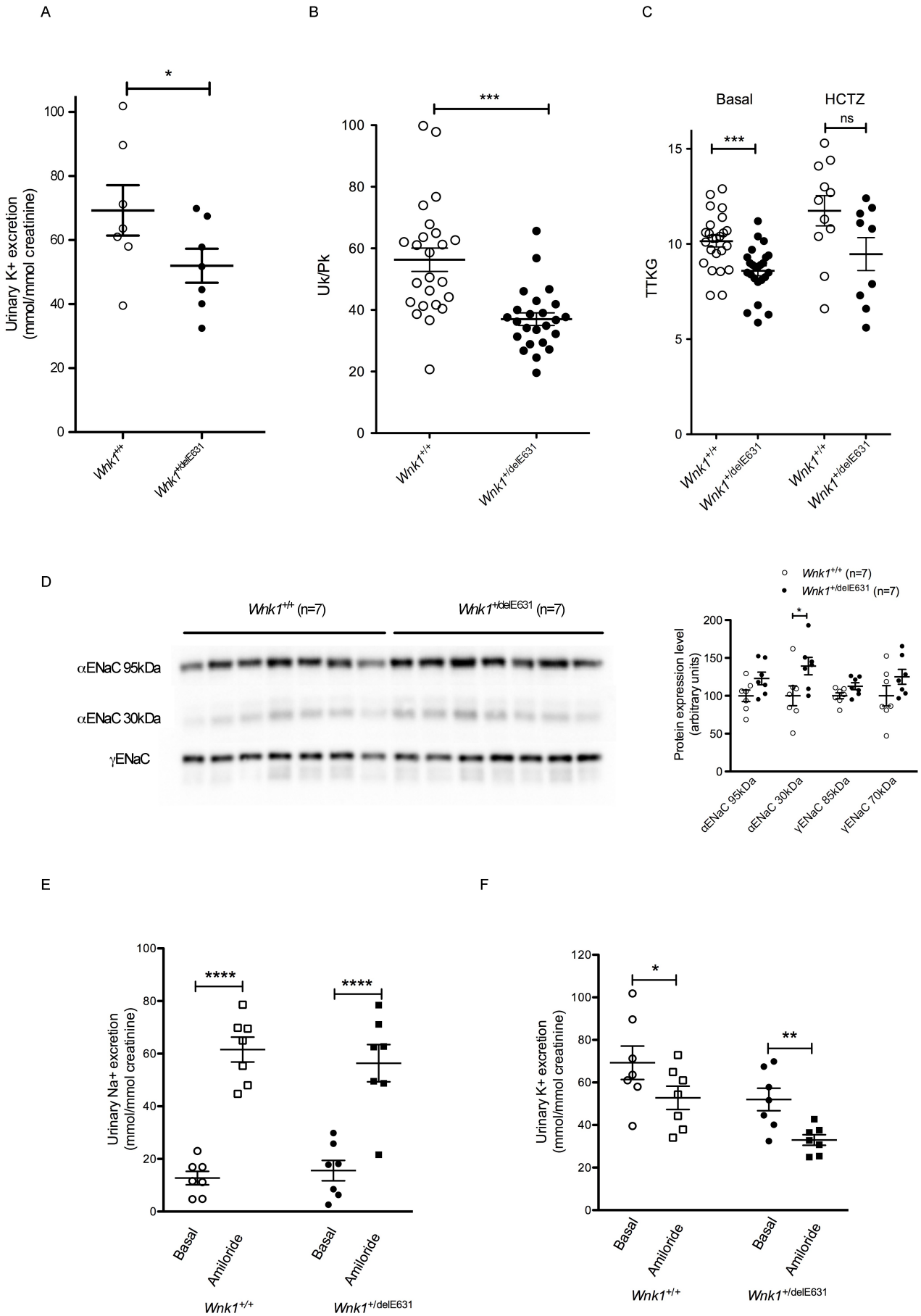
A
B
C
*
***
Basal
HCTZ
ns
***
Urinary K+ excretion (mmol/mmol creatinine)
Uk/Pk
TTKG
Wnk1+/+
Wnk1+/delE631
D
Wnk1+/+ (n=7)
Wnk1+/delE631 (n=7)
αENaC 95kDa
αENaC 30kDa
γENaC
Protein expression level (arbitrary units)
αENaC 95kDa
αENaC 30kDa
γENaC 85kDa
γENaC 70kDa
E
F
****
****
Urinary Na+ excretion (mmol/mmol creatinine)
Urinary K+ excretion (mmol/mmol creatinine)
Basal
Amiloride
Wnk1+/+
Wnk1+/delE631

Figure 8: Abnormal K+ handling in *Wnk1*$^{+/delE631}$ mice.

A-C Decreased UK^+ excretion, Uk/Pk ratio and transtubular potassium gradient (TTKG)

A.Urinary K^+ excretion was lower in *Wnk1*$^{+/delE631}$ (n=7, 52 ±5.3) than in *Wnk1*$^{+/+}$ mice (n=7, 69.3 ± 7.9, *p<0.05) (unpaired Student's t test)

B. Basal urinary/plasma ratio of K^+ concentration was lower in *Wnk1*$^{+/delE631}$ (n=24, 37.2 ±2.1) than in *Wnk1*$^{+/+}$ mice (n=24, 56.3 ± 3.8, ***p<0.001) (unpaired Student's t test)

C. TTKG was significantly lower in *Wnk1*$^{+/delE631}$ (n=24, 8.6 ±0.3) than in *Wnk1*$^{+/+}$ mice (n=24, 10.1 ±0.3, ***p=0.0003). Following a 4-day HCTZ oral (240 mg/kg/d) administration, the difference of TTKG between *Wnk1*$^{+/+}$ and *Wnk1*$^{+/delE631}$ remained the same (9.5±0.9 versus 11.8±0.8 respectively) although no more significant (p=0.068), likely because of the lower number of animals studied (n=9 and n=11, respectively). Statistical comparisons were made using unpaired t tests.

D : ENaC expression Representative immunoblots with the indicated antibodies performed on the membrane-enriched fractions of the renal cortex of mice of each genotype. Densitometric analysis. The abundance of the cleaved form of the α-subunit of ENaC was significantly increased in *Wnk1*$^{+/delE631}$ mice compared to *Wnk1*$^{+/+}$ mice. The expression level in *Wnk1*$^{+/+}$ mice was arbitrarily set to 100. Values are means ± SEM..**p<0.05*. (unpaired Student's t test)

E-F Natriuretic and kaliuretic response to amiloride

Urinary Na^+ (E) and K^+ (F) excretion in response to amiloride injection. *Wnk1*$^{+/+}$ and *Wnk1*$^{+/delE631}$ males (n=7 in each group) were housed in metabolic cages and received one injection of vehicle or amiloride on 2 consecutive days. Urines were collected 6 hours after the injection. Data are means ± SEM. *p<0.05, ***p*< 0.01, ****p<0.0001 versus the vehicle (unpaired Student's t test)

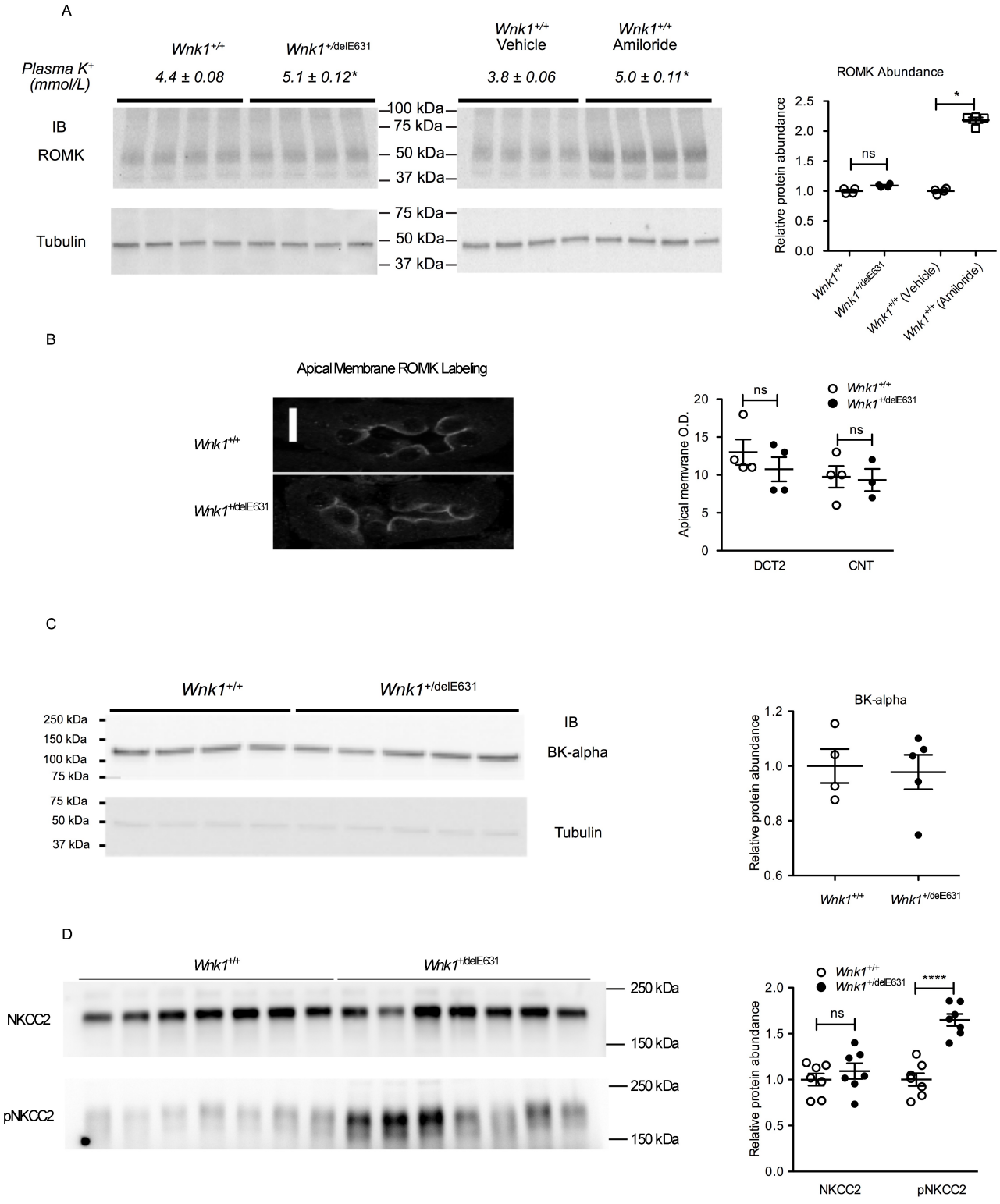

Figure 9. Expression of ROMK, BK channel and NKCC2

A. ROMK protein abundance

No change in cortical ROMK expression was observed in *Wnk1*$^{+/delE631}$ (n=4) vs littermates *Wnk1*$^{+/+}$ (n=4) mice, despite the latter group having a significantly higher plasma K^+ levels (4.4±0.08 mM, n= 20 vs. 5.1±0.12 mM, n= 20). Conversely, a more than a 2-fold increase was observed in *Wnk1*$^{+/+}$ mice treated by amiloride (25mg/kg/d for 4 days) achieving a similar rise in plasma potassium (*Wnk1*$^{+/+}$ vehicle: 3.8±0.06 mM, n=4 vs.

Wnk1$^{+/+}$ amiloride: 5.0±0.11mM). Quantification of cortical ROMK expression (n=4 per group; significance determined by t-test with * = $p<0.05$)

B. ROMK Immunofluorescence in the distal tubule

Upper part : Immunolocalization of ROMK in the DCT2 of *Wnk1*$^{+/+}$ and *Wnk1*$^{+/delE631}$ mice

Lower part :. Analysis of membrane labeling intensity showed no change ROMK apical expression in the DCT2 and CNT of *Wnk1*$^{+/delE631}$ mice (n=4 animals per genotype)

C. Basal BK alpha channel protein abundance in *Wnk1*$^{+/delE631}$ mice and *Wnk1*$^{+/+}$ littermates

BK-alpha immunoblots (upper panel) and quantification (lower panel) demonstrate that cortical BK-alpha expression is unchanged between W*nk*1$^{+/+}$ (n=4) and W*nk*1$^{+/delE631}$ mice (n=5).

D. Basal NKCC2 and P-NKCC2 protein abundance in *Wnk1*$^{+/delE631}$ mice and *Wnk1*$^{+/+}$ littermates. (n=7 per group)

NKCC2 and pNKCC2 immunoblots (upper panel) and quantification (lower panel) demonstrate that NKCC expression is unchanged between W*nk*1$^{+/+}$ (n=7) and W*nk*1$^{+/delE631}$ mice (n=7), but pNKCC2 is significantly increased (**** $p<0.0001$) in W*nk*1$^{+/delE631}$ mice compared to W*nk*1$^{+/+}$. (unpaired Student's t test).

Table 1: Basic clinical and biochemical characteristics of index cases with *WNK1* exon 7 missense variants

Id	Mutation	Age (years)	Sex (F/M)	BMI (kg/m^2)	SBP (mmHg)	DBP (mmHg)	Na (mmol/L)	K (mmol/L)	Cl (mmol/L)	CO_2t (mmol/L)	Creatinine* (umol/L)	Renin (mU/L)	Aldo (pmol/L).	UAG$ (pmol/L)	Urinary Ca/creat**
K3-1	Q636R	25	F	32.0	148	116	140	5.5	108	20	77	< 5	227	54	0.4
K29-1	D635E	47	F	23.1	104	70	136	5.7	102	21	62	2.4	53	50	0.7
K30-1	D635E	0.6	M	14.2	95	55	139	6.4	108	17	47	-	-	-	-
K58-1	A634T	13	F	19.9	105	55	140	6.0	111	21	46	3.9	132	-	0.2
K73-1	Q636E	14	M	20.1	138	80	142	5.0	109	-	79	<1	521	-	0.3
K75-1	A634T	32	F	18.6	117	85	141	5.1	110	21	58	3.5	75	136	0.7
K76-1	Q636R	27	M	20.9	134	81	144	6.4	112	24	85	<0.1 ***	219	-	-
K88-1	A634T	22	F	19.2	148	100	140	7.1	107	19	54	< 0.2 ***	1385	59	0.7
K91-1	D635N	2.5	M	19.4	90	60	139	6.3	103	20	36	0.1 ***	226	15	0.4
Mean		20		20.8	120	78	140	5.9	108	20	60	3.3 £	315	63	0.5
SD		15		4.8	23	21	2	0.7	3	2	17	0.8 £	428	45	0.2

* Creatinine reference values in children: newborn: 21-75 µmol/L; 2months- 3 years: 15-37µmol/L; 3 – 7 years 27-52 37µmol/L

** Urinary Ca/creat reference values in children: <6months: 0.10-2.6 mmol/mol; 6-12months: 0.09-2.2 mmol/mol; 1-2years:0.07-1.5 mmol/mol and 2-3years: 0.06-1.4 mmol/mol

§ UAG (urinary anion gap) represents an indirect index of urinary ammonia excretion; in normal subjects UAG should be negative during acidosis.

£ Mean and SD values calculated on plasma renin values expressed in mU/L

*** Unit in ng/ml/h

Table 2: Comparison of the main clinical and biological features of patients with missense variants at exon 7 of either the *WNK1* or the *WNK4* gene.

	WNK1 patients with Exon 7 variants				WNK4 patients with Exon 7 variants								
	Index cases	All cases	All adults	Adult males	Index Cases*	Case 1 France	Case 2 France	Case 3 France	Case 4 UK£	Case 5 China$	---------- Israeli Family # ---------- Index	Family	Males
n (M/F)	9 (4/5)	19 (7/12)	11 (3/8)	3	6 (4/2)	M	F	F	M	M	M	18 (6/12)	12
Age (years)	20±15	23±18	35±13	45±16	35±13	31	30	43	26	22	56	37±20	42±21
BMI (Kg/m^2)	21±5	20±4	22±4	22±2	28±4	28	33	24	--	--	--	--	--
SBP (mmHg)	120±23	116±20	126±18	135±10	160±18	152	180	147	150	145	185	162±30	171±20
DBP (mmHg)	78±21	73±21	86±17	90±9	98±7	100	104	87	95	95	105	99±11	103±8
HTN (Y/N)	2/7	4/15	4/7	2/3	6/0	Y	Y	Y	Y	Y	Y	12/6	12/0
K+ (mmol/L)	5.9±0.7	5.8±0.6	5.7±0.7	5.9±0.6	6.3±1.0	6.0	6.4	5.5	8.2	5.4	6.2	5.6±0.2	5.6±0.2
Cl- (mmol/L)	108±3	108±3	108±2	108±4	114±3	116	114	113	119	109	113	109±2	109±2
CO2t (mmol/L)	20±2	20±2	21±2	21±2	20±2	19	23	18	16	20	21	20±1	--
Creatinine (µmol/L)	60±17	60±16	69±12	79±5	79±19	86	62	53	106	75	123	--	--

Results as mean (1 SD) * Index cases with WNK4 mutations.
Israeli family described by Mayan et al. (58) as bearing the Q560E WNK4 mutation. All affected members had hyperkalaemia (5.2 to 6.0 mmol/L). Six out of the 18 affected subjects were normotensive, all female, but with similar biological abnormalities. Hypertension of mild to severe degree was found in most affected subjects, associated with an abnormal occurrence of stroke in our cases as well as in the family described by Mayan et al (58). Such family history of stroke was not present in any of the 9 WNK1-E7 families described here.
£ Golbang et al. Hypertension 2005; 46:295-300, D564H WNK4 mutation (59)
$ Gong et al. Endocrine 2008; 33:230-4, P561L WNK4 mutation, a 17 year old boy who developed hypertension 2 years ago, resistant to metoprolol, nifedipine and lisinopril. Blood pressure fluctuated between 140-150/ 90-100 mmHg without treatment in hospital (60)

Table 3 : Blood pressure and biological characteristics of the *Wnk1*$^{+/delE631}$ mouse model

	---------- Basal ----------			---------- HCTZ ----------		
Characteristics	***Wnk1*$^{+/+}$**	***Wnk1*$^{+/delE631}$**	**p value**	***Wnk1*$^{+/+}$**	***Wnk1*$^{+/delE631}$**	**p value**
Systolic BP (mmHg)	110.3 ±3.8 (n=11)	119.0 ±2.8 (n=12)	0.07	108.4 ±3.9 (n=11)	114.3 ±2.8 (n=12)	0.02
Blood						
Na+ (mmol/L)	144.8 ±0.2 (n=20)	145 ±0.3 (n=20)	0.61	144.5 ±0.4 (n=8)	143.3 ±0.4 (n=8)	0.05
K+ (mmol/L)	4.4 ±0.1 (n=20)	5.1 ±0.1 (n=20)	<0.0001	3.9 ±0.1 (n=8)	4.4 ±0.1 (n=8)	0.01
Cl- (mmol/L)	110.0 ±0.6 (n=20)	113.6 ±0.4 (n=20)	<0.0001	106.8 ±0.9 (n=8)	106 ±0.7 (n=8)	0.53
Renin (Units)	1.0 ±0.2 (n=7)	0.5 ±0.1 (n=7)	0.04	ND	ND	
Urine						
Aldosterone (nmol/L)	6.8 ±0.7 (n=7)	11.5 ±1.6 (n=7)	0.02	ND	ND	
Aldo/Creatinine (Units)	1.5 ±0.2 (n=7)	2.5 ±0.5 (n=7)	0.09	ND	ND	